



## GRP94 rewires and buffers the FLT3-ITD signaling network and promotes survival of acute myeloid leukemic stem cells

by Beibei Zhang, Pilar Ayuda Durán, Laure Piechaczyk, Yngvar Fløisand, Mireia Mayoral Safont Safont, Ida Tveit Karlsen, Zina Fandalyuk, Dagim Tadele, Pepijn van Mierlo, Alexander D. Rowe, Joseph M. Robertson, Bjørn Tore Gjertsen, Emmet McCormack, and Jorrit M. Enserink. Collaborative Groups: Bjørn Tore Gjertsen Group (Bjørn Tore Gjertsen), Emmet McCormack Group (Emmet McCormack)

Haematologica 2018 [Epub ahead of print]

*Citation: Beibei Zhang, Pilar Ayuda Durán, Laure Piechaczyk, Yngvar Fløisand, Mireia Mayoral Safont Safont, Ida Tveit Karlsen, Zina Fandalyuk, Dagim Tadele, Pepijn van Mierlo, Alexander D. Rowe, Joseph M. Robertson, Bjørn Tore Gjertsen, Emmet McCormack, and Jorrit M. Enserink. Collaborative Groups: Bjørn Tore Gjertsen Group (Bjørn Tore Gjertsen), Emmet McCormack Group (Emmet McCormack). GRP94 rewires and buffers the FLT3-ITD signaling network and promotes survival of acute myeloid leukemic stem cells. Haematologica. 2018; 103:xxx  
doi:10.3324/haematol.2018.189399*

### *Publisher's Disclaimer.*

*E-publishing ahead of print is increasingly important for the rapid dissemination of science. Haematologica is, therefore, E-publishing PDF files of an early version of manuscripts that have completed a regular peer review and have been accepted for publication. E-publishing of this PDF file has been approved by the authors. After having E-published Ahead of Print, manuscripts will then undergo technical and English editing, typesetting, proof correction and be presented for the authors' final approval; the final version of the manuscript will then appear in print on a regular issue of the journal. All legal disclaimers that apply to the journal also pertain to this production process.*

# **GRP94 rewires and buffers the FLT3-ITD signaling network and promotes survival of acute myeloid leukemic stem cells**

by

Beibei Zhang<sup>1,2,3</sup>, Pilar Ayuda-Durán<sup>1,2,3</sup>, Laure Piechaczyk<sup>1,2,4</sup>, Yngvar Fløisand<sup>1,2,5</sup>, Mireia Mayoral Safont<sup>6</sup>, Ida Tveit Karlsen<sup>6</sup>, Zina Fandalyuk<sup>6</sup>, Dagim Tadele<sup>1,2,4</sup>, Pepijn van Mierlo<sup>1</sup>, Alexander D. Rowe<sup>7</sup>, Joseph M. Robertson<sup>1,2</sup>, Bjørn Tore Gjertsen<sup>5,8</sup>, Emmet McCormack<sup>5,8</sup>, and Jorrit M. Enserink<sup>1,2,9,10</sup>

<sup>1</sup> Department of Molecular Cell Biology, Institute for Cancer Research, Oslo University Hospital, Montebello, 0379 Oslo, Norway

<sup>2</sup> Centre for Cancer Cell Reprogramming, Institute of Clinical Medicine, Faculty of Medicine, Montebello, 0379 Oslo, Norway

<sup>3</sup> Equal contributions

<sup>4</sup> Institute of Clinical Medicine, University of Oslo, Oslo, Norway

<sup>5</sup> Department of Hematology, Oslo University Hospital, Rikshospitalet, Oslo, Norway

<sup>6</sup> Centre for Cancer Biomarkers, Department of Clinical Science, University of Bergen, Bergen, Norway

<sup>7</sup> Norwegian National Unit for Newborn Screening, Woman and Children's Division, Oslo University Hospital, Rikshospitalet, Norway

<sup>8</sup> Hematology Section, Department of Internal Medicine, Haukeland University Hospital, Bergen, Norway

<sup>9</sup> Section for Biochemistry and Molecular Biology, The Department of Biosciences, Faculty of Mathematics and Natural Sciences, University of Oslo, Oslo, Norway

<sup>10</sup> To whom correspondence should be addressed: [jorrit.enserink@rr-research.no](mailto:jorrit.enserink@rr-research.no)

Running title: Mechanism of GRP94 addiction of AML

RETRACTED

## Abstract

Internal tandem duplications in the tyrosine kinase receptor FLT3 (FLT3-ITD) are among the most common lesions in acute myeloid leukemia and there exists a need for new forms of treatment. Using *ex vivo* drug sensitivity screening, we found that FLT3-ITD+ patient cells are particularly sensitive to HSP90 inhibitors. While it is well known that HSP90 is important for FLT3-ITD stability, we found that HSP90 family members play a much more complex role in FLT3-ITD signaling than previously appreciated. First, we found that FLT3-ITD activates the unfolded protein response, leading to increased expression of GRP94/HSP90B1. This results in activation of a nefarious feedback loop, in which GRP94 rewires FLT3-ITD signaling by binding and retaining FLT3-ITD in the endoplasmic reticulum, leading to aberrant activation of downstream signaling pathways and further inducing the unfolded protein response. Second, HSP90 family proteins protect FLT3-ITD+ acute myeloid leukemia cells against apoptosis by alleviating proteotoxic stress, and treatment with HSP90 inhibitors results in proteotoxic overload that triggers unfolded protein response-induced apoptosis. Importantly, leukemic stem cells are strongly dependent upon HSP90 for their survival, and the HSP90 inhibitor ganetespib causes leukemic stem cell exhaustion in patient-derived mouse xenograft models. Taken together, our study reveals a molecular basis for HSP90 addiction of FLT3-ITD+ acute myeloid leukemia cells and provides a rationale for including HSP90 inhibitors in the treatment regime for FLT3-ITD+ acute myeloid leukemia.

Keywords: FLT3/Acute myeloid leukemia/HSP90/ER stress/leukemic stem cells

## Introduction

Treatment of acute myeloid leukemia (AML) has not changed significantly during the past decades. AML is a heterogeneous disease, and over 100 unique combinations of known or suspected oncogenic mutations have been identified<sup>1</sup>, suggesting that specific subtypes of AML require specific treatment regimens. Activating mutations in *FLT3* have been observed in approximately 30% of AMLs<sup>1</sup>, and detection of the FLT3-ITD mutation at first diagnosis is associated with increased risk of relapse and poor clinical outcome<sup>2</sup>.

Interestingly, FLT3-ITD is partially retained as an immature protein in intracellular compartments including the endoplasmic reticulum (ER), and this aberrant localization is important for activation of several downstream pathways required for tumor cell proliferation and survival, such as STAT3 and STAT5<sup>3, 4</sup>. However, the underlying molecular mechanism that prevents FLT3-ITD from maturing and translocating to the cell membrane remains unknown.

In AML, small populations of self-renewing leukemic stem cells (LSCs) generate the bulk of leukemic cells<sup>5</sup>. LSCs are relatively resistant to chemotherapy and persist as a potential source of relapse. Expression of FLT3-ITD increases the risk of relapse<sup>6</sup>, suggesting it promotes LSC, and drugs that eradicate LSCs may provide more durable remission than standard chemotherapy. Several tyrosine kinase inhibitors (TKIs) are in development as targeted therapy for FLT3-mutated AML. Unfortunately, FLT3-ITD TKIs only have a relatively modest and transient effect<sup>7</sup>, indicating that TKIs do not completely eradicate LSCs. TKI resistance can occur as a result of mutations in the kinase domain of FLT3, particularly residue D835 and the

gatekeeper residue F691<sup>8</sup>. Intrinsic cellular pathways can also modulate TKI resistance<sup>9</sup>, yet the nature of these pathways remains poorly understood. Identifying these pathways, as well as the cellular mechanisms that enable FLT3-ITD to drive uncontrolled cell proliferation and survival, may help identify vulnerabilities in the AML network that can be therapeutically exploited.

The heat shock protein 90 (HSP90) family of molecular chaperones is important for stabilizing and activating many cell signaling proteins under normal conditions<sup>10</sup>. Human cells express four HSP90 members, i.e. HSP90 $\alpha$  and HSP90 $\beta$ , glucose-regulated protein 94 (GRP94), and tumor necrosis factor receptor-associated protein 1 (TRAP1). HSP90 $\alpha$  and HSP90 $\beta$  (collectively referred as “HSP90” hereafter) are mainly cytosolic, whereas GRP94 is found in the ER and TRAP1 in mitochondria<sup>11</sup>. In addition to its chaperoning functions under normal conditions, HSP90 family proteins also mediate adaptive responses to stress, serving as a crucial facilitator of oncogene addiction and cancer cell survival<sup>10</sup>. For instance, HSP90 protects oncoproteins from misfolding and degradation<sup>10</sup>. Furthermore, the increased rate of protein synthesis induced by oncogenic signaling frequently induces proteotoxic stress, and HSP90 family proteins are essential for mitigating this stress to promote tumor cell survival.

Proteotoxic stress typically results in accumulation of unfolded proteins in the ER, which triggers the unfolded protein response (UPR<sup>12</sup>). The UPR restores cell homeostasis by degrading misfolded proteins and by inducing the synthesis of chaperones, including GRP94<sup>13</sup>. The UPR consists of three main signaling pathways: the kinase IRE1 $\alpha$ ; the kinase PERK; and the transcription factor Atf6<sup>12</sup>. Although the UPR promotes cell survival under mild proteotoxic stress, it triggers apoptosis after prolonged and excessive ER stress<sup>12</sup>. Under these conditions,

the IRE1 $\alpha$  and ATF6 pathways are inactivated, while PERK signaling is maintained<sup>14</sup>. PERK signaling can generate high levels of reactive oxygen species (ROS), which triggers apoptosis<sup>15</sup>. While increased ROS production, ER stress, and activation of the UPR have been observed in many different human cancers, including AML<sup>16</sup>, it is currently unclear whether there exists a physiologically relevant link between FLT3-ITD, HSP90, ER stress and ROS.

In this study, we reveal a molecular basis for HSP90 addiction of FLT3-ITD-driven AML cells, and provide a rationale for treatment FLT3-ITD+ AML with HSP90 inhibitors.

## Methods

### *Cells*

Bone marrow (BM) derived blast cells were purified by density gradient centrifugation from patients and healthy donors and cultured in Mononuclear Cell Medium (PromoCell). RS4;11, MV4-11 and Ba/F3 cells were obtained from DSMZ. RS4;11 cells were maintained in RPMI1640 medium, MV4-11 cells in IMDM with 2 mM L-Glutamine and Ba/F3 cells in RPMI1640 medium with 0.75 ng/ml recombinant mouse IL-3. Medium for all cell lines was supplemented with 10% heat-inactivated FBS, 100U penicillin G/ml and 100  $\mu$ g /ml streptomycin.

### *Patient cohort*

AML patients were diagnosed, sampled and treated at the Department of Hematology, Oslo University Hospital, Norway. Samples were collected from 41 AML patients and 6 healthy

volunteers after obtaining written informed consent. The study was approved by the ethical review board (REK Sør-øst 2015-1012) in accordance with the Declaration of Helsinki.

#### *Cell transfection and siRNA*

Ba/F3 cells were transfected with pCRU5-Flt3-AB-IRES-GFP or pCRU5-Flt3-ITD-IRES-GFP, pLKO.1-blast-FLT3-ITD or pLKO.1-blast-FLT3-ITD-D835V/D835Y/D835F/F691L (kindly provided by Prof. C. Récher), using Amaxa Nucleofector II Device (Lonza) or Lipofectamine 3000 according to the manufacturer's instructions. siRNA for *GRP94* and control siRNA (Santa Cruz Biotechnology) were transfected using Lipofectamine RNAiMAX.

#### *Immunofluorescence staining and confocal fluorescent Microscopy*

The plasma membrane of poly-L-lysine-immobilized cells was stained on ice with whole-wheat germ agglutinin conjugated to AlexaFluor488. Cells were fixed with 4% formaldehyde for 10 min and permeabilized with ice-cold 0.5% Triton X-100 PBS for 4 min, washed 3 times with PBS and blocked 15 min at RT (PBS with 0.5% BSA). Cells were incubated with primary antibodies at 4°C overnight, washed and stained for 1 h with fluorophore-conjugated secondary antibodies at RT, after which cells were washed, mounted (Vector laboratories) and examined by confocal microscopy (Leica) at RT. Fluorescent images were collected with the Leica Application Suite X (LASX1.1.0.12420) and processed with Adobe Photoshop and Illustrator.

#### *Mouse PDX studies*

T-cell-depleted or CD34<sup>+</sup> selected human AML cells from a chemotherapy-refractory FLT3-ITD<sup>+</sup> AML patient were transplanted into 8-week-old NOD.Cg-Prkdcscid IL2rgtm1Wjl/SzJ



mice (NSG mice, University of Bergen, Norway) as previously described <sup>17</sup>. After engraftment was confirmed, mice were treated with either vehicle ( $n = 11$ ) or ganetespib (100 mg/kg, Q2W, i.v.;  $n = 11$ ) for 3 weeks. A group of mice ( $n = 8$  per group) was followed for survival after discontinuation of treatment. BM cells from primary recipients were used for secondary transplantation into NSG mice ( $n = 3$  per group) following completion of treatment, and engraftment was analyzed for survival. Mouse care and experimental procedures were performed in accordance with approved protocols from the Norwegian Animal Research Authority in accordance with The European Convention for the Protection of Vertebrates Used for Scientific Purposes.

### *Statistics*

Significant differences between two groups were determined with Student's *t*-test. All data were expressed as the mean  $\pm$  standard error of the mean (SEM). A *p* value smaller than 0.05 was considered significant. Survival data was analyzed using the Kaplan and Meier method. The Mantel-Haenzel log-rank statistics (GraphPad Prism 5.0, GraphPad Software) was used to analyze survival distribution.

## Results

### *HSP90 inhibitors are among the most potent drugs that target FLT3-ITD-positive AML blasts*

We tested the sensitivity of blast cells of 41 AML patients against 349 drugs with anticancer activity by *ex vivo* drug screening<sup>18</sup>, using the response of bone marrow (BM) cells from six healthy donors as control (see Supplemental Tables S1 and S2 for compounds and patient information). We calculated drug sensitivity scores using the Drug Hunter app (see Supplemental Methods). Clustering analysis revealed that AML patients with FLT3-ITD or FLT3-TKD mutations tended to co-cluster with a subset of drugs that included the HSP90 inhibitors luminespib/AUY922 and ganetespib/STA9090 (Fig. 1A and Fig. S1A). Indeed, AML cells expressing high levels of FLT3-ITD (cut-off: at least 20% FLT3-ITD-positive blasts in BM) were significantly more sensitive to ganetespib and luminespib than cells expressing wild-type FLT3 (FLT3-WT; Fig. 1B,C). The same was observed for patients with FLT3-TKD mutations (Fig. 1B,C). Although cell proliferation rates were reduced, BM cells from healthy donors tolerated very high doses of ganetespib and luminespib (1-10  $\mu$ M; Suppl. Fig. S1B-E), suggesting the existence of a therapeutic window.

These data show that FLT3-mutant AML is associated with a unique *ex vivo* drug sensitivity profile, and that FLT3-mutant AML blasts are particularly sensitive to HSP90 inhibitors.

### *The FLT3-ITD-specific proteome includes HSP90 family members*

To better understand HSP90 inhibitor sensitivity, and to gain insight into the molecular mechanisms that underpin FLT3-ITD-driven cell proliferation, we immunoprecipitated FLT3 and FLT3-ITD from RS4;11 cells and MV4-11 cells, which exclusively express FLT3-WT and

FLT3-ITD, respectively <sup>19</sup>, and identified co-immunoprecipitating proteins by mass spectrometry (MS; Fig. 2A and Suppl. Table S3). We identified several proteins previously known to bind FLT3, including JAK1, Grb2, DOCK2 and Bruton tyrosine kinase (BTK) <sup>20-22</sup>, of which both Grb2 and BTK were significantly enriched in the FLT3-ITD fraction (Fig. 2A). Gene Ontology analysis of the FLT3-ITD-specific MS dataset revealed that proteins involved in protein folding were highly overrepresented in the FLT3-ITD-specific fraction ( $p \leq 1.07E-06$ ; Fig. 2B and C), and STRING analysis revealed that FLT3-ITD associates with a molecular chaperone network (Fig. 2D). Interestingly, this chaperone network includes multiple HSP90 family proteins, and subsequent co-immunoprecipitation experiments confirmed several FLT3-ITD-specific interactions, including HSP90 (Fig. 2E), GRP94 (Fig. 2F), and the ER chaperone Calnexin (Suppl. Fig. S2A). Similar data were obtained with isogenic Ba/F3 cells expressing FLT3-WT or FLT3-ITD as well as primary AML cells (data not shown and Fig. 2G and H). These experiments show that FLT3-ITD is part of a rewired protein interaction network that includes HSP90 family members.

#### *The HSP90 family member GRP94 is required for ER retention of FLT3-ITD*

FLT3-ITD has been shown to aberrantly localize to the ER as an immature protein, but the molecular mechanism is unknown. First, we confirmed that FLT3-ITD is indeed present in the ER by analyzing the localization of FLT3 in MV4-11 cells and in RS4;11 cells (Fig. 3A,B; Suppl. Fig. S2B). The same localization patterns were observed in isogenic Ba/F3 cells (Suppl. Fig. S2C; <sup>23</sup>), demonstrating that mislocalization of FLT3-ITD is intrinsic to FLT3-ITD and not due to an unrelated defect in the genetic background of MV4-11 cells. In agreement with a previous study <sup>24</sup>, failure of FLT3-ITD to translocate to the cell surface was accompanied by a

pronounced glycosylation defect (Suppl. Fig. S2D), showing that ER-localized FLT3-ITD is a hypoglycosylated, immature protein. Consistently, FLT3-ITD was not downregulated upon treatment with its ligand FLT3L (Suppl. Fig. S2E), which is a known consequence of cell membrane-localized FLT3-WT stimulation (Suppl. Fig. S2F; <sup>25</sup>). Maturation and cell surface expression of FLT3-ITD was restored by treatment with the FLT3 inhibitor AC220/quizartinib (Suppl. Fig. S2E and G, Suppl. Fig. S3A; <sup>23</sup>), implying that aberrant ER localization is caused by constitutive FLT3-ITD activity. Together, these data confirm that FLT3-ITD is largely retained in the ER.

We hypothesized that binding to GRP94 might contribute to ER retention of FLT3-ITD, because GRP94 is primarily localized to the ER lumen, and because GRP94 is important for folding of cell surface receptors <sup>26</sup>. Moreover, GRP94 is known to sustain certain hematopoietic malignancies <sup>27</sup>. We inhibited GRP94 either by depletion with siRNA or by treatment with the GRP94-selective inhibitor PU-WS13 <sup>28</sup>. Interestingly, GRP94 inhibition resulted in maturation and cell surface translocation of FLT3-ITD (Fig. 3C,D; Suppl. Fig. S3B,F), even though total cell surface expression of FLT3-ITD was slightly reduced after prolonged treatment (Suppl. Fig. S3A). Similar results were obtained with isogenic Ba/F3 cells (Suppl. Fig. S3C). Treatment with the broad-range HSP90 inhibitor ganetespib <sup>29</sup> also resulted in a relative increase in cell membrane localization (Suppl. Fig. S3D), although prolonged exposure resulted in a dramatic reduction in total FLT3-ITD levels (Suppl. Fig. S3A,D; also see below). The effect of HSP90 inhibitors was not a cell line peculiarity, because ganetespib also induced cell membrane localization of FLT3-ITD in primary AML patient cells (Fig. 3E,F). These data show that HSP90 proteins, particularly GRP94, are responsible for retaining FLT3-ITD in the ER.

### *GRP94 is required for FLT3-ITD signaling competence*

We further explored the importance of the interaction between FLT3-ITD and GRP94, and found that the maturation of FLT3-ITD induced by GRP94 inhibition was accompanied by a substantial reduction in phosphorylation of the downstream targets STAT5 and AKT/PKB (Fig. 4A, Suppl. Fig. S3E)<sup>30, 31</sup>. This was somewhat unexpected, because AKT is classically thought to be activated at the plasma membrane rather than the ER. However, recent reports have shown that there exists a substantial intracellular pool of AKT at endosomes and the ER<sup>32-34</sup>, which might be activated by FLT3-ITD. Consistently, GRP94 inhibition resulted in degradation of the downstream AKT signaling pathway component  $\beta$ -catenin (Fig. 4A), leading to reduced expression of several  $\beta$ -catenin target genes, such as *CCND1*, *MYC* and *CD44* (Fig. 4B). Similar findings were obtained with ganetespib, although in contrast to GRP94 inhibitors, which did not have a strong effect on the protein levels of FLT3-ITD, ganetespib induced a strong reduction in FLT3-ITD levels (Fig. 4C). Furthermore, a luciferase-based reporter assay showed that ganetespib was a more potent inhibitor of STAT5 than the direct STAT5 inhibitor STAT5i (*N'*-((4-oxo-4H-chromen-3-yl)methylene)nicotinohydrazide)<sup>35</sup> (Fig. 4D). Similar data were obtained with BM cells derived from an FLT3-ITD+ AML patient, whereas signaling in blast cells from an FLT3-WT AML patient was unaffected (Fig. 4E).

Taken together, these data indicate that different HSP90 family members have multiple effects on FLT3-ITD; HSP90 is required for FLT3-ITD stability, whereas GRP94 retains FLT3-ITD in the ER where it abnormally engages downstream signaling pathways.

### *FLT3-ITD signaling activates the UPR*

Hyperactivation of oncogenic signaling pathways is frequently associated with increased protein synthesis, elevated ROS levels and accumulation of misfolded proteins in the ER, and the resulting ER stress is an emerging hallmark of cancer<sup>36</sup>. ER stress is a potent UPR stimulus, and one of the consequences of UPR activation is increased expression of *HSP90B1*, the gene encoding GRP94<sup>37</sup>. Furthermore, cells gauge the quality of protein folding by the degree of protein glycosylation<sup>37</sup>. Given that FLT3-ITD is hyperactive and hypoglycosylated (Suppl. Fig. S2D), we hypothesized that FLT3-ITD triggers the UPR. Indeed, we found that transcription of *HSP90B1* as well as GRP94 protein levels were significantly higher in cells expressing FLT3-ITD than in FLT3-WT cells (Fig. 5A,B). GRP94 levels were reduced by AC220, indicating that increased GRP94 expression is caused by aberrant FLT3-ITD activity (Fig. S4A). GRP94 protein levels were also increased in patient-derived FLT3-ITD+ cells compared with BM cells obtained from either FLT3-WT AML patients or healthy donors (Fig. 5C, Suppl. Fig. S4B). FLT3-ITD+ cells also had higher ROS levels (Suppl. Fig. S4C), which is another ER stress indicator<sup>37</sup>. We therefore analyzed the activity of several UPR signaling pathways, and found that FLT3-ITD+ cells indeed have higher phosphorylation levels of IRE1 $\alpha$  and PERK, as well as relatively increased processing of XBP1 and Atf6 (Fig. 5D and S4D). Similar findings were obtained with isogenic Ba/F3 cells (Suppl. Fig. S4E). These data indicate that the UPR is activated in FLT3-ITD+ AML cells.

#### *HSP90 protects FLT3-ITD-expressing cells against ROS and PERK-dependent cell death*

Next, we determined the role of HSP90 in activation of the UPR by FLT3-ITD. Treatment of MV4-11 cells with either PU-WS13 or ganetespib resulted in rapid dephosphorylation of IRE1 $\alpha$  and loss of cleaved Xbp1 and Atf6 (Fig. 5E, Suppl. Fig. S4F). In

contrast, PERK phosphorylation was much more sustained, indicating that HSP90 inhibitors induce a switch from cytoprotective UPR to pro-apoptotic UPR<sup>14</sup>. Similar findings were obtained with FLT3-ITD+ Ba/F3 cells and with primary FLT3-ITD+ AML cells, whereas no such effects were observed with healthy BM cells (Suppl. Fig. S4G-I). Sustained PERK activity induces ROS and triggers apoptosis<sup>15</sup>; consistently, upon inhibition of GRP94 we observed a significant increase in ROS levels and apoptosis (5F,G; Suppl. Fig. S4J-M). Conversely, the ROS scavenger N-acetyl cysteine (NAC) strongly reduced ROS levels and significantly improved survival of PU-WS13-treated cells (Suppl. Fig. S4M, Fig. 5H), indicating that inhibition of GRP94 results in ROS-mediated apoptosis. Finally, the PERK inhibitor GSK2606414<sup>38</sup> protected against ganetespib-induced cell death (Fig. 5I), confirming that PERK triggers cell death in response to HSP90 inhibitors.

Taken together, these data indicate that HSP90 proteins protect FLT3-ITD-expressing cells against FLT3-ITD-induced ER stress and UPR-mediated cell death.

#### *HSP90 inhibitors synergize with TKIs and bypass TKI-resistant mutations in FLT3-ITD*

A major drawback of targeted therapies is that their effect is generally only partial and transient<sup>39</sup>. Our data suggest that HSP90 family proteins might be relevant targets for combination treatment of FLT3-ITD+ AML. To explore this idea, we treated cells expressing FLT3-WT or FLT3-ITD with PU-WS13 and monitored cell survival. PU-WS13 had little effect on survival of FLT3-WT-expressing RS4;11 cells, but it significantly reduced cell survival of FLT3-ITD-expressing MV4-11 cells (Fig. 6A). More importantly, PU-WS13 enhanced the ability of the FLT3 TKI AC220 to selectively kill FLT3-ITD-expressing cells (Fig. 6A,B), indicating that GRP94 increases the TKI tolerance of FLT3-ITD-expressing cells. In-depth

analysis of the combination of these drugs with SynergyFinder<sup>40</sup> demonstrated that they synergized in killing FLT3-ITD+ cells (Suppl. Fig. S5A-D). Depletion of GRP94 by siRNA also potentiated the effect of AC220 (Fig. 6C). Furthermore, a combination of AC220 and HSP90 inhibitors had only a minor effect on healthy BM cells and on AML cells expressing FLT3-WT, whereas viability of FLT3-ITD-positive blasts was significantly reduced by treatment for 72 hrs with AC220 in combination with a low dose of either PU-WS13 or ganetespib (Fig. 6D,E; Suppl. Fig. S5E). We also performed long-term cell proliferation assays to test the durability of the combination of AC220 with HSP90 inhibitors. Mock-treated cells increased 4000-fold compared to day 1 (Fig. 6F), and treatment with a low, sub-lethal dose (5 nM) of ganetespib reduced cell proliferation by approximately 50% (Fig. 6F). Although AC220 by itself was initially very effective at blocking cell proliferation, ultimately a fraction of cells resumed proliferation, leading to a >500-fold increase in cell numbers after 28 days compared to the start of the experiment (Fig. 6F). However, combination of AC220 with ganetespib completely prevented TKI escape.

A major problem with targeted therapies is development of resistance, and identification of drugs that bypass TKI resistance would be a major advance in AML treatment. The most common clinically observed mechanism of TKI resistance involves mutation of the D835 or the F691 residue in the FLT3 kinase domain<sup>41,42</sup>. We created Ba/F3 cell lines expressing FLT3-ITD with a D835V, D835Y, D835F or F691L mutation, and tested their sensitivity to AC220, PU-WS13 and ganetespib. As expected, these mutations conferred complete AC220 resistance compared with Ba/F3 cells expressing FLT3-ITD lacking these mutations (Fig. 6G). However, viability of these mutants, especially the highly TKI-resistant FLT3-ITD-D835Y/F mutants<sup>41</sup>,



was significantly reduced by both PU-WS13 and ganetespib (Fig. 6G). Some of these mutants showed increased sensitivity to HSP90 inhibitors, suggesting that drug-resistant forms of FLT3-ITD increase cellular dependency on HSP90. Together, these data show that HSP90 inhibitors may be a powerful asset in treatment of drug-resistant FLT3-ITD+ AML.

#### *Inhibition of HSP90 selectively eradicates FLT3-ITD+ LSCs*

Since we found that ganetespib blocks the activity of STAT5 and  $\beta$ -catenin, which both play an important role in LSC survival<sup>43, 44</sup>, we tested the effect of ganetespib on LSCs. We isolated BM cells from three FLT3-WT AML patients and from three FLT3-ITD+ AML patients, treated them with ganetespib, and analyzed the relative number of cells in the CD34+ CD38- and CD34+ CD38- CD123+ compartments, which are known to contain LSCs<sup>45, 46</sup>. Strikingly, although the number of cells with these LSC markers was significantly higher in FLT3-ITD+ AML than in FLT3-WT AML-derived BM (Fig. 7A,B), ganetespib treatment resulted in almost complete eradication of FLT3-ITD+ LSCs. CD34+CD38-CD123+ cells derived from FLT3-WT AML patients were sensitive to ganetespib as well, indicating that ganetespib may broadly impair survival of CD34+CD38-CD123+ AML cells. Similar findings were obtained with cells expressing the LSC markers CD96 and CLL-1<sup>47, 48</sup> (Fig. 7C-E). Thus, FLT3-ITD+ LSCs are highly dependent upon HSP90 activity.

We evaluated the efficacy of ganetespib in a zebrafish animal model (Fig. 7F). Treatment with ganetespib or AC220 resulted in a significant decrease in transplanted MV4-11 cells, without causing major side effects on the fish (Suppl. Fig. S6A,B). The effect of these drugs was also tested in a patient-derived xenograft (PDX) zebrafish model. FLT3-ITD+ AML blasts had

the tendency to aggressively spread throughout the fish and in some cases even killed the host (Fig. 7G and Suppl. Fig. S6C,D), but treatment with ganetespib significantly reduced tumor size and promoted fish survival (Fig. 7G-I and S6C,D). These compounds had little or no effect on BM cells transplanted from a healthy donor (Fig. S6E,F) or on blasts derived from a FLT3-WT AML patient (Suppl. Fig. S6G,H).

Encouraged by these data, we tested the effect of ganetespib on an FLT3-ITD<sup>+</sup> mouse model (Fig. 7J). As shown in Figure 7K, treatment with ganetespib significantly improved survival of the mice compared to controls ( $p < 0.0001$ ). Ganetespib also significantly enhanced survival after secondary transplantation of BM cells from mice that received ganetespib treatment (Fig. 7L), suggesting that brief treatment with HSP90 inhibitors leads to a reduction or exhaustion of the LSC pool. Together, these data show that there exists a therapeutic window for HSP90 inhibitors and that HSP90 inhibitors may target LSCs *in vivo*.

## Discussion

In this study, we screened for drugs that may benefit specific patient subpopulations and discovered that FLT3-ITD+ AML cells are sensitive to a range of compounds, particularly HSP90 inhibitors. We unraveled the molecular basis for HSP90 addiction of FLT3-ITD-expressing cells, and found that FLT3-ITD activates the UPR, leading to increased expression of GRP94 (see Fig. 7M for a model). GRP94 then establishes a nefarious feedback loop by physically interacting with FLT3-ITD, resulting in retention of FLT3-ITD in the ER where it aberrantly engages signaling pathways that promote tumor cell survival and which may further increase proteotoxic stress<sup>3, 36</sup>. Importantly, selective inhibition of GRP94 causes maturation and cell membrane localization, thereby breaking the nefarious feedback loop (Fig. 7N). This uncouples FLT3-ITD from downstream signaling pathways, resulting in diminished cell proliferation and survival. It is presently not entirely clear why GRP94 and other HSP90 proteins associate with FLT3-ITD. It is possible that ITD mutations alter the overall structure of FLT3-ITD, interfering with folding of FLT3-ITD such that it is recognized by HSP90 family proteins.

While HSP90 is known to be important for FLT3-ITD stability, our data suggest a much more complex role for HSP90 family proteins in FLT3-ITD signaling. There appears to be a division of labor in this process; GRP94 retains FLT3-ITD in the ER, whereas other HSP90 proteins, most likely HSP90 $\alpha$  and HSP90 $\beta$ , are important for stabilizing FLT3-ITD and for mitigating proteotoxic stress caused by oncogenic FLT3-ITD activity. We propose a model in which inhibition of HSP90 causes proteotoxic ER stress overload, overwhelming the UPR and triggering PERK-mediated cell death (Fig. 7N). Indeed, we found that a small-molecule inhibitor of PERK suppressed HSP90 inhibitor-induced cell death. It is important to note that, perhaps

paradoxically, HSP90 inhibitors trigger apoptosis while simultaneously inducing the destruction of FLT3-ITD. One explanation for this paradox is that proteostasis in tumor cells is extremely fragile <sup>49</sup>, and that HSP90 inhibitors cause rapid and long-lasting accumulation of unfolded proteins in FLT3-ITD-expressing cells, leading to irreversible commitment to apoptosis even as FLT3-ITD is being degraded.

The results from our study provide a rationale for treatment of FLT3-ITD+ AML with HSP90 inhibitors. While clinical application of first-generation HSP90 inhibitors was hampered by severe toxicity, phase I/II clinical trials have demonstrated that ganetespib is safe and well tolerated <sup>50</sup>. In addition to FLT3-ITD, ganetespib also effectively targeted FLT3-ITD cells with secondary TKD mutations, which is important because these mutations can confer TKI resistance <sup>8,41</sup>. This indicates that HSP90 inhibitors may have the ability to delay or even prevent development of TKI resistance. Further support for using HSP90 inhibitors in clinical settings comes from our finding that ganetespib effectively eradicated FLT3-ITD+ LSCs *ex vivo*, and that brief HSP90 inhibitor treatment delayed the onset of leukemia in a mouse LSC assay, indicating that HSP90 inhibitors have the potential to reduce or exhaust the FLT3-ITD+ LSC pool *in vivo*. This is important, because chemotherapy-resistant LSCs are a source of relapse after treatment.

In conclusion, our study reveals a previously undescribed molecular basis for HSP90 addiction of FLT3-ITD-driven AML, and provides a rationale for treatment of FLT3-ITD+ AML with HSP90 inhibitors.

## **Acknowledgments**

We thank Dr. K. Wennerberg and Dr. K. Porkka for assistance with *ex vivo* drug screening and for sharing unpublished data, and the Advanced Light Microscopy core facility at Oslo University Hospital. This project was supported by grants from the Norwegian Health Authority South-East (2014014, 2012012) and the Norwegian Cancer Society (project numbers 3311782, 4487303, 144176, 6786517, 182524). The research leading to these results also received funding from the European Union Seventh Framework Programme (FP7-PEOPLE-2013-COFUND) under grant agreement n° 609020 - Scientia Fellows. This work was partly supported by the Research Council of Norway through its Centres of Excellence funding scheme, project number 262652. The authors declare no competing financial interests.

## **Author contributions**

JME conceived the study; BBZ, PAD, LP, MMS, ITK, ZF, YF, DT, PvM, AR, JMR, performed experiments; BBZ, PAD, LP, AR, JMR, BTG, EM, YF and JME analyzed the data; BBZ and JME wrote the manuscript.

## **Submission of data to public databases**

The mass spectrometry proteomics data have been deposited to the ProteomeXchange Consortium via the PRIDE partner repository with the dataset identifier PXD009423.

## **Conflict of interest**

The authors declare no conflict of interest

RETRACTED

## References

1. Cancer Genome Atlas Research N. Genomic and epigenomic landscapes of adult de novo acute myeloid leukemia. *N Engl J Med*. 2013;368(22):2059-2074.
2. Abu-Duhier FM, Goodeve AC, Wilson GA, et al. FLT3 internal tandem duplication mutations in adult acute myeloid leukaemia define a high-risk group. *Br J Haematol*. 2000;111(1):190-195.
3. Choudhary C, Olsen JV, Brandts C, et al. Mislocalized activation of oncogenic RTKs switches downstream signaling outcomes. *Mol Cell*. 2009;36(2):326-339.
4. Schmidt-Arras D, Bohmer SA, Koch S, et al. Anchoring of FLT3 in the endoplasmic reticulum alters signaling quality. *Blood*. 2009;113(15):3568-3576.
5. Bonnet D, Dick JE. Human acute myeloid leukemia is organized as a hierarchy that originates from a primitive hematopoietic cell. *Nat Med*. 1997;3(7):730-737.
6. Port M, Bottcher M, Thol F, et al. Prognostic significance of FLT3 internal tandem duplication, nucleophosmin 1, and CEBPA gene mutations for acute myeloid leukemia patients with normal karyotype and younger than 60 years: a systematic review and meta-analysis. *Ann Hematol*. 2014;93(8):1279-1286.
7. Gallogly MM, Lazarus HM. Midostaurin: an emerging treatment for acute myeloid leukemia patients. *J Blood Med*. 2016;7(73-83).
8. Smith CC, Wang Q, Chin CS, et al. Validation of ITD mutations in FLT3 as a therapeutic target in human acute myeloid leukaemia. *Nature*. 2012;485(7397):260-263.
9. Green AS, Maciel TT, Hospital MA, et al. Pim kinases modulate resistance to FLT3 tyrosine kinase inhibitors in FLT3-ITD acute myeloid leukemia. *Sci Adv*. 2015;1(8):e1500221.
10. Trepel J, Mollapour M, Giaccone G, Neckers L. Targeting the dynamic HSP90 complex in cancer. *Nat Rev Cancer*. 2010;10(8):537-549.
11. Taldone T, Ochiana SO, Patel PD, Chiosis G. Selective targeting of the stress chaperome as a therapeutic strategy. *Trends Pharmacol Sci*. 2014;35(11):592-603.
12. Hetz C. The unfolded protein response: controlling cell fate decisions under ER stress and beyond. *Nat Rev Mol Cell Biol*. 2012;13(2):89-102.
13. Marzec M, Eletto D, Argon Y. GRP94: An HSP90-like protein specialized for protein folding and quality control in the endoplasmic reticulum. *Biochim Biophys Acta*. 2012;1823(3):774-787.
14. Lin JH, Li H, Yasumura D, et al. IRE1 signaling affects cell fate during the unfolded protein response. *Science*. 2007;318(5852):944-949.
15. Han J, Back SH, Hur J, et al. ER-stress-induced transcriptional regulation increases protein synthesis leading to cell death. *Nat Cell Biol*. 2013;15(5):481-490.
16. Sun H, Lin DC, Guo X, et al. Inhibition of IRE1alpha-driven pro-survival pathways is a promising therapeutic application in acute myeloid leukemia. *Oncotarget*. 2016;7(14):18736-18749.
17. Li L, Osdal T, Ho Y, et al. SIRT1 activation by a c-MYC oncogenic network promotes the maintenance and drug resistance of human FLT3-ITD acute myeloid leukemia stem cells. *Cell Stem Cell*. 2014;15(4):431-446.
18. Pemovska T, Kontro M, Yadav B, et al. Individualized systems medicine strategy to tailor treatments for patients with chemorefractory acute myeloid leukemia. *Cancer Discov*. 2013;3(12):1416-1429.

19. Quentmeier H, Reinhardt J, Zaborski M, Drexler HG. FLT3 mutations in acute myeloid leukemia cell lines. *Leukemia*. 2003;17(1):120-124.
20. Wu M, Hamaker M, Li L, Small D, Duffield AS. DOCK2 interacts with FLT3 and modulates the survival of FLT3-expressing leukemia cells. *Leukemia*. 2017;31(3):688-696.
21. Oellerich T, Mohr S, Corso J, et al. FLT3-ITD and TLR9 use Bruton tyrosine kinase to activate distinct transcriptional programs mediating AML cell survival and proliferation. *Blood*. 2015;125(12):1936-1947.
22. Zhang S, Mantel C, Broxmeyer HE. Flt3 signaling involves tyrosyl-phosphorylation of SHP-2 and SHIP and their association with Grb2 and Shc in Baf3/Flt3 cells. *J Leukoc Biol*. 1999;65(3):372-380.
23. Reiter K, Polzer H, Krupka C, et al. Tyrosine kinase inhibition increases the cell surface localization of FLT3-ITD and enhances FLT3-directed immunotherapy of acute myeloid leukemia. *Leukemia*. 2018;32(2):313-322.
24. Williams AB, Li L, Nguyen B, Brown P, Levis M, Small D. Fluvastatin inhibits FLT3 glycosylation in human and murine cells and prolongs survival of mice with FLT3/ITD leukemia. *Blood*. 2012;120(15):3069-3079.
25. Turner AM, Lin NL, Issarachai S, Lyman SD, Broudy VC. FLT3 receptor expression on the surface of normal and malignant human hematopoietic cells. *Blood*. 1996;88(9):3383-3390.
26. Randow F, Seed B. Endoplasmic reticulum chaperone gp96 is required for innate immunity but not cell viability. *Nat Cell Biol*. 2001;3(10):891-896.
27. Hua Y, White-Gilbertson S, Kellner J, et al. Molecular chaperone gp96 is a novel therapeutic target of multiple myeloma. *Clin Cancer Res*. 2013;19(22):6242-6251.
28. Patel PD, Yan P, Seidler PM, et al. Paralog-selective Hsp90 inhibitors define tumor-specific regulation of HER2. *Nat Chem Biol*. 2013;9(11):677-684.
29. Taldone T, Patel PD, Patel M, et al. Experimental and structural testing module to analyze paralogue-specificity and affinity in the Hsp90 inhibitors series. *J Med Chem*. 2013;56(17):6803-6818.
30. Brandts CH, Sargin B, Rode M, et al. Constitutive activation of Akt by Flt3 internal tandem duplications is necessary for increased survival, proliferation, and myeloid transformation. *Cancer Res*. 2005;65(21):9643-9650.
31. Mizuki M, Fenski R, Halfter H, et al. Flt3 mutations from patients with acute myeloid leukemia induce transformation of 32D cells mediated by the Ras and STAT5 pathways. *Blood*. 2000;96(12):3907-3914.
32. Giorgi C, Ito K, Lin HK, et al. PML regulates apoptosis at endoplasmic reticulum by modulating calcium release. *Science*. 2010;330(6008):1247-1251.
33. Schenck A, Goto-Silva L, Collinet C, et al. The endosomal protein Appl1 mediates Akt substrate specificity and cell survival in vertebrate development. *Cell*. 2008;133(3):486-497.
34. Betz C, Stracka D, Prescianotto-Baschong C, Frieden M, Demaux N, Hall MN. Feature Article: mTOR complex 2-Akt signaling at mitochondria-associated endoplasmic reticulum membranes (MAM) regulates mitochondrial physiology. *Proc Natl Acad Sci U S A*. 2013;110(31):12526-12534.
35. Muller J, Sperl B, Reindl W, Kiessling A, Berg T. Discovery of chromone-based inhibitors of the transcription factor STAT5. *Chembiochem*. 2008;9(5):723-727.



36. Dai C, Dai S, Cao J. Proteotoxic stress of cancer: implication of the heat-shock response in oncogenesis. *J Cell Physiol.* 2012;227(8):2982-2987.
37. Wang M, Kaufman RJ. The impact of the endoplasmic reticulum protein-folding environment on cancer development. *Nat Rev Cancer.* 2014;14(9):581-597.
38. Axten JM, Medina JR, Feng Y, et al. Discovery of 7-methyl-5-(1-([3-(trifluoromethyl)phenyl]acetyl)-2,3-dihydro-1H-indol-5-yl)-7H-pyrrolo[2,3-d]pyrimidin-4-amine (GSK2606414), a potent and selective first-in-class inhibitor of protein kinase R (PKR)-like endoplasmic reticulum kinase (PERK). *J Med Chem.* 2012;55(16):7193-7207.
39. Hanahan D. Rethinking the war on cancer. *Lancet.* 2014;383(9916):558-563.
40. Ianevski A, He L, Aittokallio T, Tang J. SynergyFinder: a web application for analyzing drug combination dose-response matrix data. *Bioinformatics.* 2017;33(15):2413-2415.
41. Smith CC, Lin K, Stecula A, Sali A, Shah NP. FLT3 D835 mutations confer differential resistance to type II FLT3 inhibitors. *Leukemia.* 2015;29(12):2390-2392.
42. Albers C, Leischner H, Verbeek M, et al. The secondary FLT3-ITD F691L mutation induces resistance to AC220 in FLT3-ITD+ AML but retains in vitro sensitivity to PKC412 and Sunitinib. *Leukemia.* 2013;27(6):1416-1418.
43. Yoshimoto G, Miyamoto T, Jabbarzadeh-Tabrizi S, et al. FLT3-ITD up-regulates MCL-1 to promote survival of stem cells in acute myeloid leukemia via FLT3-ITD-specific STAT5 activation. *Blood.* 2009;114(24):5034-5043.
44. Wang Y, Krivtsov AV, Sinha AU, et al. The Wnt/beta-catenin pathway is required for the development of leukemia stem cells in AML. *Science.* 2010;327(5973):1650-1653.
45. Lapidot T, Sirard C, Vormoor J, et al. A cell initiating human acute myeloid leukaemia after transplantation into SCID mice. *Nature.* 1994;367(6464):645-648.
46. Jin L, Lee EM, Ramshaw HS, et al. Monoclonal antibody-mediated targeting of CD123, IL-3 receptor alpha chain, eliminates human acute myeloid leukemic stem cells. *Cell Stem Cell.* 2009;5(1):31-42.
47. Hosen N, Park CY, Tatsumi N, et al. CD96 is a leukemic stem cell-specific marker in human acute myeloid leukemia. *Proc Natl Acad Sci U S A.* 2007;104(26):11008-11013.
48. van Rhenen A, van Dongen GA, Kelder A, et al. The novel AML stem cell associated antigen CLL-1 aids in discrimination between normal and leukemic stem cells. *Blood.* 2007;110(7):2659-2666.
49. Dai C, Sampson SB. HSF1: Guardian of Proteostasis in Cancer. *Trends Cell Biol.* 2016;26(1):17-28.
50. Ramalingam S, Goss G, Rosell R, et al. A randomized phase II study of ganetespib, a heat shock protein 90 inhibitor, in combination with docetaxel in second-line therapy of advanced non-small cell lung cancer (GALAXY-1). *Ann Oncol.* 2015;26(8):1741-1748.

## Figure legends

**Figure 1. *Ex vivo* drug sensitivity testing reveals that HSP90 inhibitors are among the most potent inhibitors of FLT3-mutant AML.** *A*, Hierarchical clustering analysis of 41 AML patients against the drug library. Clustering was performed using the area-under-curve values as described in the Methods section. *B, C*, HSP90 inhibitors selectively inhibit FLT3-mutant AML. The graphs show ganetespib (*B*) and luminespib (*C*) sensitivity of BM cells derived from healthy donors (HD), and patients with FLT3-WT AML, FLT3-ITD<sup>+</sup> AML, and FLT3-TKD AML. Coloring indicates the relative expression levels of FLT3-ITD.

**Figure 2. The interactome of FLT3-ITD includes HSP90 family members.** *A*, Volcano plot indicating differences between the proteomes of FLT3-WT and FLT3-ITD. See Suppl. Table S3 for the complete list. *B*, Metascape analysis of the proteins that preferentially interact with FLT3-ITD. *C*, GO-Slim Biological Process analysis of the FLT3-ITD protein interaction network. *D*, FLT3-ITD is associated with a network of molecular chaperones. The network was visualized by STRING analysis. *E, F*, FLT3-ITD but not FLT3-WT interacts with HSP90 and GRP94. FLT3 and FLT3-ITD were immunoprecipitated from RS4;11 cells (FLT3-WT) and MV4-11 cells (FLT3-ITD), respectively, and copurifying proteins were analyzed by Western blotting using antibodies against HSP90 $\alpha/\beta$  (*E*) and GRP94 (*F*). *G, H*, FLT3-ITD but FLT3-WT interacts with HSP90 and GRP94 in primary patient samples. The experiment was performed as described in (*E, F*) using cells derived from patient 32 (FLT3-WT AML) or patient 23 (FLT3-ITD<sup>+</sup> AML).

**Figure 3. GRP94 retains FLT3-ITD in the ER.** **A**, Localization of FLT3-WT and FLT3-ITD. RS4;11 cells (FLT3-WT) and MV4-11 cells (exclusively FLT3-ITD) were fixed, permeabilized and stained with DAPI, Alexa Fluor 488-conjugated wheat germ agglutinin to stain the cell membrane, and anti-FLT3 antibodies. **B**, Quantification of the data shown in panel (A). Three independent experiments were performed. Error bars, SEM. \*\*,  $p < 0.01$ . **C**, Inhibiting GRP94 induces cell membrane translocation of FLT3-ITD. GRP94 was inhibited by siRNA or by treatment with 50  $\mu$ M PU-WS13 for 24 hrs, and the nucleus, the cell membrane and FLT3 were visualized as described in (A). GRP94 protein levels of siRNA-treated cells are shown in Suppl. Figure S3F. **D**, Quantification of the data shown in panel (C). Three independent experiments were performed. Error bars, SEM. \*\*,  $p < 0.01$ . **E**, Treatment with ganetespib induces cell membrane translocation of FLT3-ITD in primary patient samples. BM-derived cells from a healthy donor or an FLT3-ITD+ AML patient were treated with 50 nM ganetespib for 24 hrs after which FLT3 was visualized as described in (A). **F**, Quantification of the data shown in panel (E). Three independent experiments were performed. Error bars, SEM. NS, not significant; \*\*,  $p < 0.01$ .

**Figure 4. HSP90 family proteins are required for FLT3-ITD signaling competence.** **A**, Inhibition of GRP94 attenuates FLT3-ITD signaling in MV4-11 cells. GRP94 was inhibited by treatment with either 50  $\mu$ M PU-WS13 for 24 hrs or by siRNA depletion and cell lysates were analyzed by Western blotting using the indicated antibodies. **B**, GRP94 activity is required for expression of  $\beta$ -catenin target genes. MV4-11 cells were treated as in (A) and expression of the indicated genes was analyzed by RT-qPCR. All values were normalized to *ACTB* mRNA levels. Three independent experiments were performed. Error bars, SEM. \*\*,  $p < 0.01$ . **C**, Ganetespib

induces degradation of FLT3-ITD and diminishes FLT3-ITD signaling. MV4-11 cells were treated with 100 nM ganetespib for the indicated times and cell lysates were analyzed by Western blotting using the indicated antibodies. **D**, Ganetespib blocks STAT5 transcriptional activity. Ba/F3 cells stably expressing FLT3-ITD, Cypridina luciferase under control of five copies of the STAT5 response element (“5xSTAT5-RE”), as well as red firefly luciferase (“rFirefly”) under control of the CMV promoter, were treated with the indicated compounds for 4 hrs after which Cypridina and rFirefly luciferase activity were analyzed as described in the Methods. Four independent experiments were performed. Error bars, SEM. \*,  $p < 0.05$ ; \*\*,  $p < 0.01$ ; \*\*\*,  $p < 0.001$ . **E**, Ganetespib inhibits FLT3 signaling in FLT3-ITD+ patient cells but not in cells derived from AML patients expressing FLT3-WT. BM-derived cells ( $1 \times 10^6$ ) were treated with 100 nM ganetespib for the indicated times and cell lysates were analyzed by Western blotting using the indicated antibodies. Blast count: 37% for patient 23 and 45% for patient 32.

**Figure 5. HSP90 family members suppress the UPR and protect cells against apoptosis. A**, *HSP90B1/GRP94* mRNA expression levels are increased in FLT3-ITD-expressing cells. mRNA levels were analyzed by RT-qPCR in three independent experiments. The value was normalized to *ACTB* mRNA levels. Error bars, SEM. \*,  $p < 0.05$ . **B**, GRP94 protein expression levels are increased in FLT3-ITD+ cells. GRP94 levels in RS4;11 and MV4-11 cells were analyzed by flow cytometry using GRP94-specific antibodies. MFI, median fluorescence intensity. **C**, GRP94 expression levels are increased in FLT3-ITD+ patient cells compared with FLT3-WT patient cells. GRP94 levels were analyzed as in (B). **D**, Activation of the UPR in FLT3-ITD-expressing cells. Cell lysates were analyzed with the indicated antibodies. **E**, Inhibition of GRP94 leads to

inactivation of the IRE1 $\alpha$  and Atf6 pathways but not the PERK pathway of the UPR. MV4-11 cells were treated with 50  $\mu$ M PU-WS13 after which cell lysates were analyzed with the indicated antibodies. **F**, Inhibiting GRP94 increases cellular ROS production in MV4-11 cells. GRP94 was inhibited by siRNA knockdown or by treatment with 50  $\mu$ M PU-WS13 and ROS was quantified by fluorescence microscopy as described in the Methods. Three independent experiments were performed. Error bars, SEM. \*\*,  $p < 0.01$ . **G**, GRP94 protects against apoptosis. Apoptosis was measured by quantifying the relative amount of apoptotic MV4-11 cells using the TUNEL assay (Suppl. Fig. S4J). Three independent experiments were performed. Error bars, SEM. \*\*,  $p < 0.01$ . **H**, Reducing cellular ROS levels with NAC significantly increases viability of PU-WS13-treated MV4-11 cells. Cells were treated for 24 hrs with 50  $\mu$ M PU-WS13 and 5 mM NAC as indicated, after which cell viability was assayed by CellTiter-Glo. Three independent experiments were performed. Error bars, SEM. \*\*,  $p < 0.01$ . **I**, Inhibition of PERK suppresses ganetespib-induced loss of cell viability. MV4-11 cells were treated with either DMSO or 20  $\mu$ M GSK2606414 in combination with increasing doses ganetespib for 48 hrs, after which cell viability was determined with CellTiter-Glo. Four independent experiments were performed. Error bars, SEM. \*\*,  $p < 0.01$ .

**Figure 6. HSP90 inhibitors synergize with FLT3 TKIs and bypass drug resistance.** **A**, PU-WS13 cooperates with AC220 to inhibit survival of FLT3-ITD-expressing cells. Cells were treated with vehicle, 50  $\mu$ M PU-WS13, 1  $\mu$ M AC220, or a combination of both drugs for 24 hrs after which cell viability was measured using CellTiter-Glo. Four independent experiments were performed. NS, not significant; Error bars, SEM. \*\*,  $p < 0.01$ . **B**, PU-WS13 synergizes with AC220 *in vitro*. MV4-11 cells were treated with an increasing dose of AC220 in combination

with either vehicle or with 50  $\mu$ M PU-WS13, after which cell viability was assayed with CellTiter-Glo. Four independent experiments were performed. Error bars, SEM. **C**, Knockdown of GRP94 sensitizes FLT3-ITD-expressing cells to AC220. MV4-11 cells were transfected with control siRNA or GRP94 siRNA and treated with either vehicle or 1  $\mu$ M AC220 for 48 h, after which cell viability was assayed with CellTiter-Glo. Four independent experiments were performed. Error bars, SEM. \*\*,  $p < 0.01$ . **D, E**, HSP90 inhibitors sensitize patient-derived FLT3-ITD+ AML cells to AC220. BM cells ( $5 \times 10^3$  cells) from either a healthy donor or from an FLT3-ITD+ AML patient were treated with vehicle, 100 nM AC220, 5  $\mu$ M PU-WS13 (D) or 5 nM ganetespib (E), or a combination of compounds as indicated below the graphs. After 72 hrs relative cell viability was determined by CellTiter-Glo. Four independent experiments were performed. Error bars, SEM. \*,  $p < 0.05$ ; \*\*,  $p < 0.01$ . Blast count patient AML-5: 60%. **F**, Ganetespib prevents TKI escape of FLT3-ITD+ cells.  $1 \times 10^4$  MV4-11 cells were treated with vehicle, ganetespib, AC220, or a combination of ganetespib and AC220 for the indicated times after which cell proliferation was determined by counting cell numbers. Cells were replated three times per week in fresh medium with the relevant inhibitors to maintain constant cell counts. The experiments were performed in triplicates. Error bars, SEM. \*\*,  $p < 0.01$ . **G**, Ganetespib bypasses drug resistance. Ba/F3 cells stably expressing normal FLT3-ITD or various clinically relevant TKI-resistant FLT3-ITD kinase mutants were treated with the indicated doses of AC220, PU-WS13 or ganetespib for 24 hrs after which cell viability was determined by CellTiter-Glo. Four independent experiments were performed. Error bars, SEM. \*,  $p < 0.05$ ; \*\*,  $p < 0.01$ .

**Figure 7. HSP90 inhibitors target FLT3-ITD+ LSCs. A-E**, BM cells ( $1 \times 10^6$  cells) from three FLT3-WT AML patients and from three FLT3-ITD+ AML patients were purified by

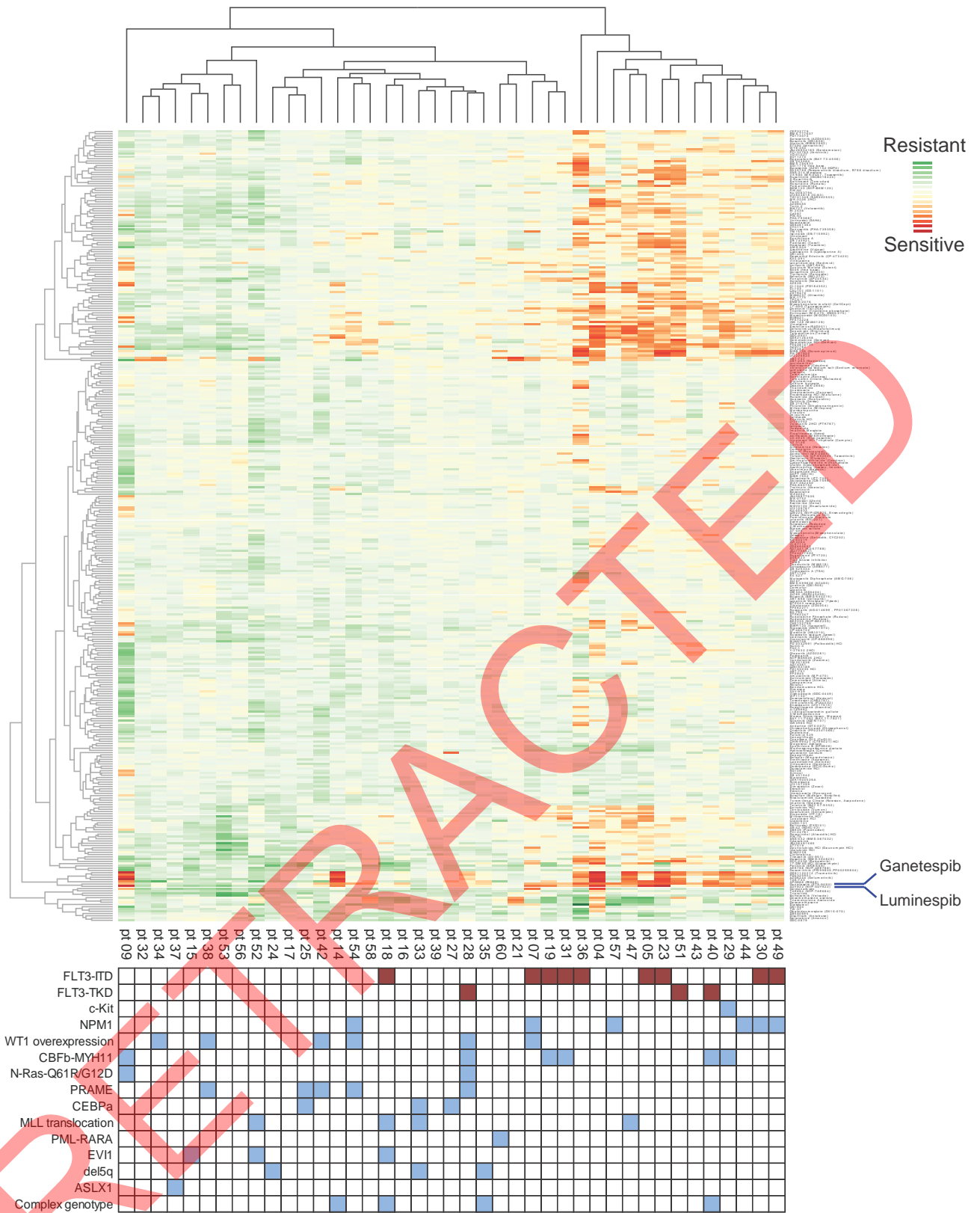
gradient centrifugation and treated with 100 nM ganetespib for the indicated times, after which the percentage of cells in these samples were analyzed by flow cytometry for expression of CD34<sup>+</sup>CD38<sup>-</sup> (A), CD34<sup>+</sup> CD38<sup>-</sup> CD123<sup>+</sup> (B), CD96<sup>+</sup> (C), CLL-1<sup>+</sup> (D) and CD96<sup>+</sup> CLL-1<sup>+</sup> (E). All values were normalized to the untreated FLT3-WT AML samples. Three independent experiments were performed. Error bars, SEM. Blast counts for the three FLT3-WT samples: 45% (of which 45% CD34<sup>+</sup>), 70-75% (of which 29% CD34<sup>+</sup>), and 20% (30% CD34<sup>+</sup>); blast counts for the three FLT3-ITD<sup>+</sup> samples: 40% (37% CD34<sup>+</sup>), 24% (with 24% CD34<sup>+</sup> cells) and an undetermined blast count with 87% CD34<sup>+</sup> cells. **F**, Experimental set-up of zebrafish PDX experiments. **G**, Ganetespib inhibits FLT3-ITD<sup>+</sup> AML cells in a zebrafish PDX model. Xenografted zebrafish were treated with DMSO, 100 nM AC220, 100 nM ganetespib, or a combination of drugs, and AML cells were visualized by fluorescence microscopy. **H**, Quantification of the relative tumor sizes shown in (G). Error bars, SEM. \*,  $p < 0.05$ ; \*\*,  $p < 0.01$ . **I**, Relative survival of the fish in the experiment shown in (G). 10-15 fish were analyzed for each treatment and three independent experiments were performed. NS, not significant; Error bars, SEM. \*,  $p < 0.05$ ; \*\*,  $p < 0.01$ . **J**, Set-up of the mouse PDX experiments. **K**, CD34<sup>+</sup> cells from a FLT3-ITD<sup>+</sup> AML patient were injected into NSG mice and treated for 3 weeks with vehicle or ganetespib (see Methods). The graph indicates survival of the mice after discontinuation of treatment. **L**, HSP90 promotes survival of LSCs. Graph shows survival of secondary recipients after transplantation of BM cells from mice treated with either vehicle or ganetespib. **M**, Model for HSP90 addiction of FLT3-ITD<sup>+</sup> AML cells. FLT3-ITD causes mild proteotoxic stress, which activates the UPR leading to increased GRP94 expression. GRP94 then sets up a feedback loop that boosts FLT3-ITD signaling capacity by binding and retaining FLT3-ITD in the ER. The FLT3-ITD-induced proteotoxic stress is alleviated by HSP90, which forms the basis for HSP90

addiction. *N*, Treatment with HSP90 inhibitors breaks the feedback loop, while simultaneously overwhelming the cell with proteotoxic stress, causing PERK-mediated apoptosis.

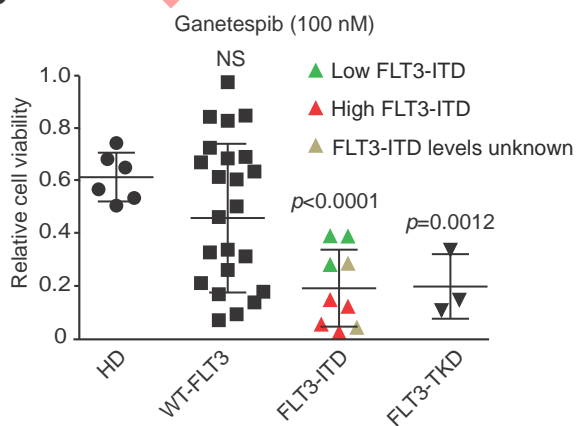
RETRACTED



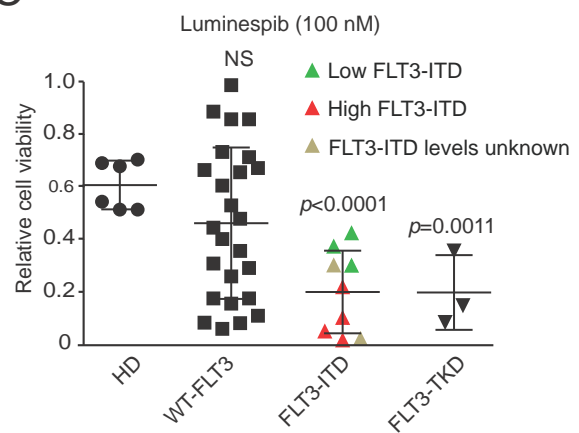
A

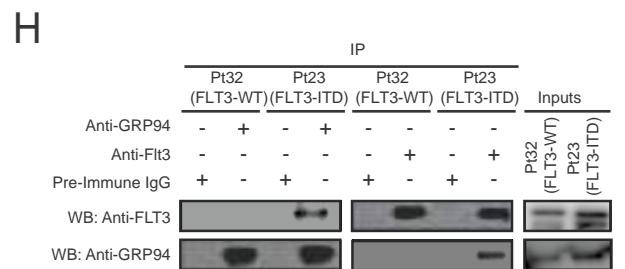
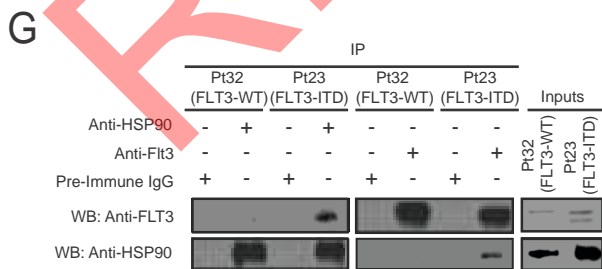
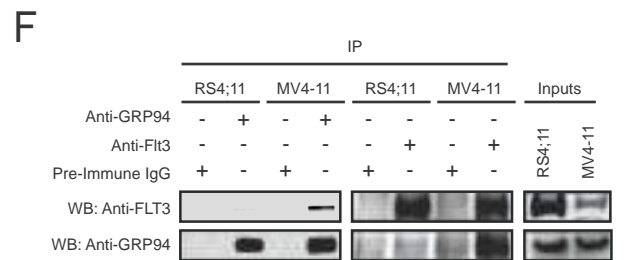
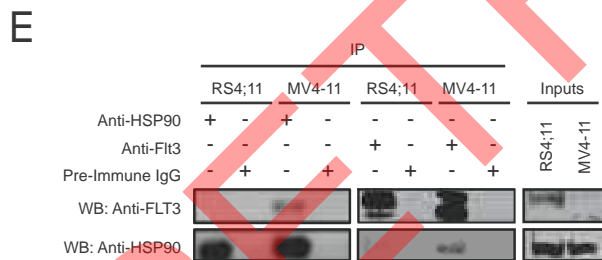
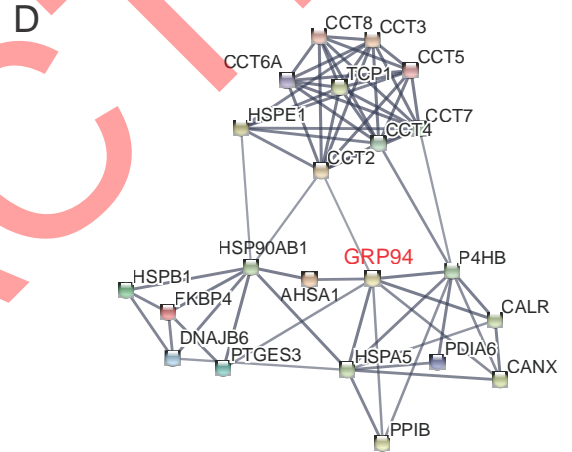
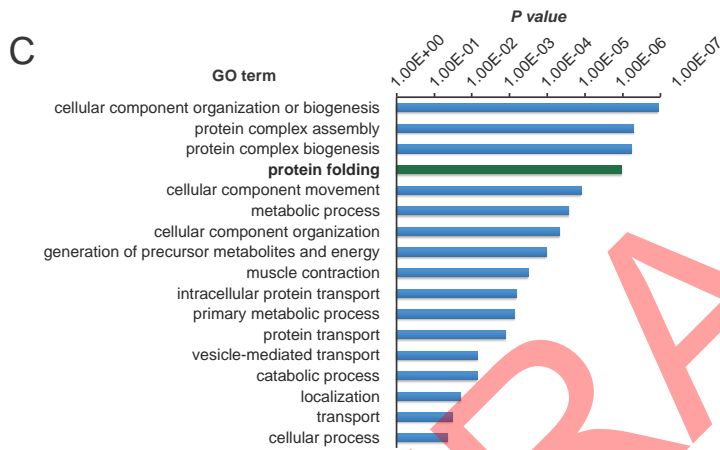
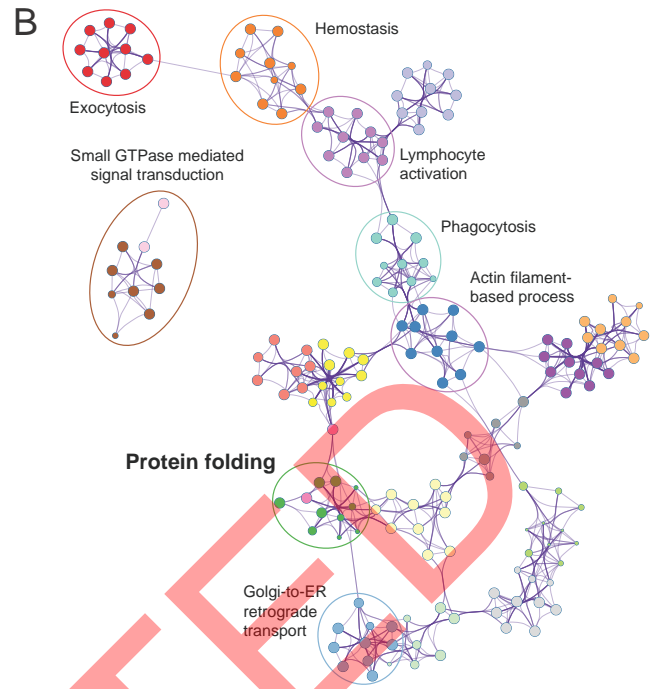
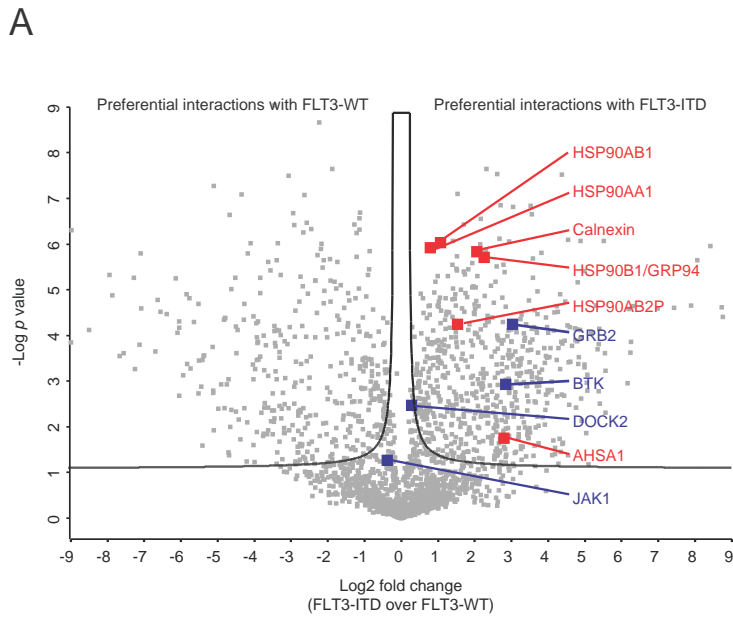


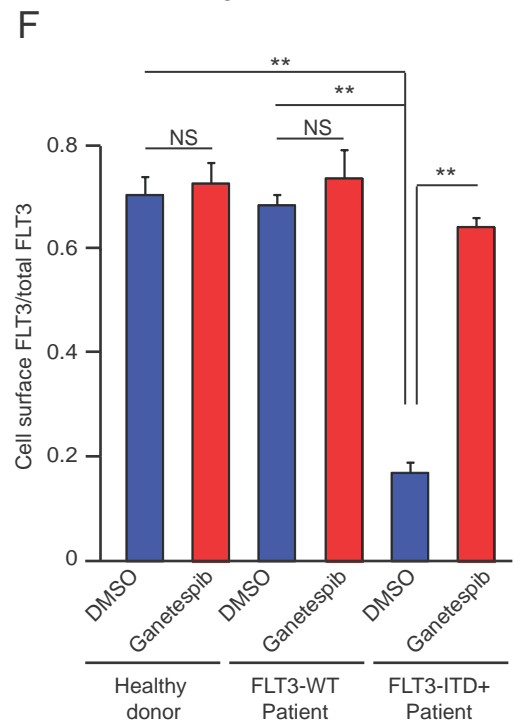
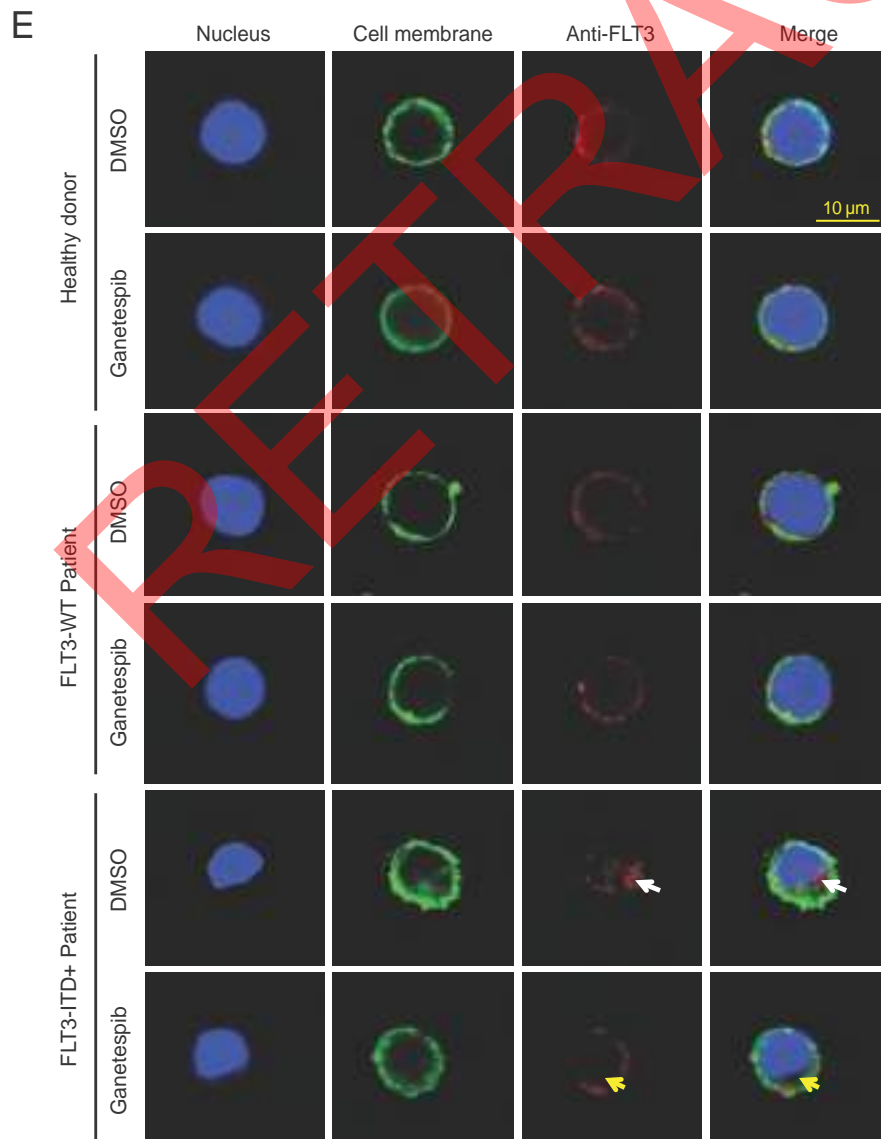
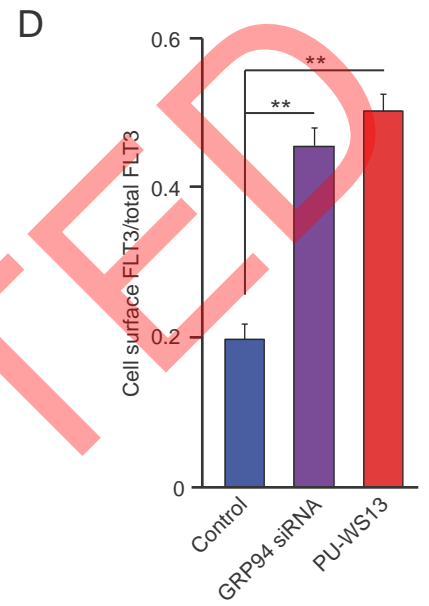
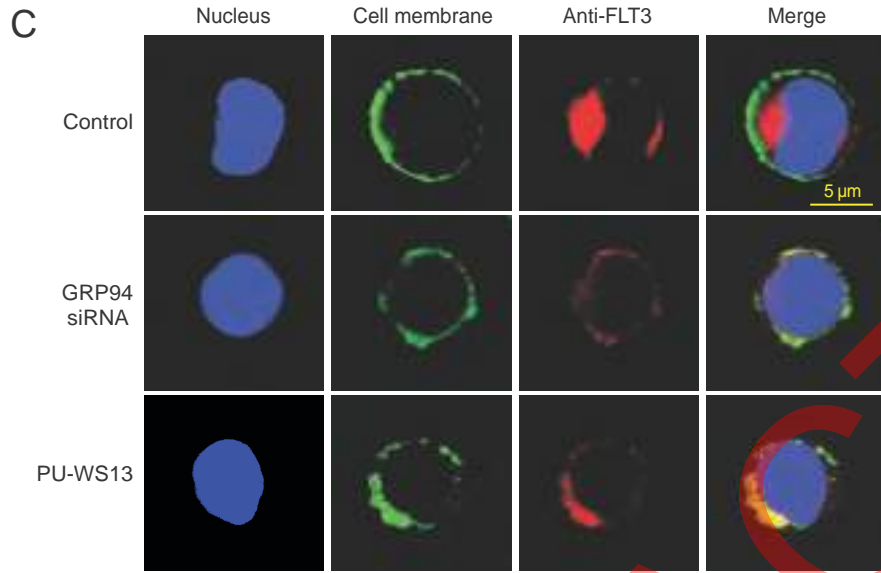
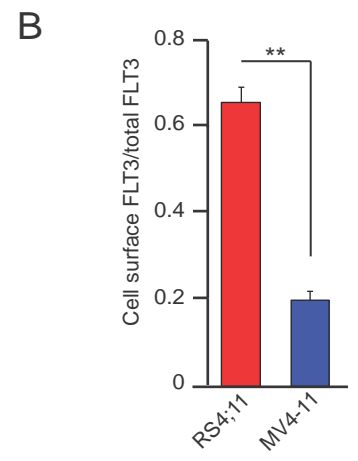
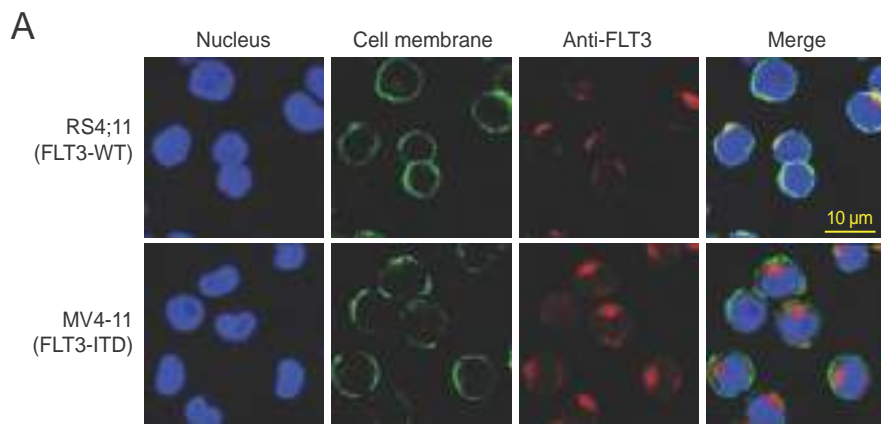
B



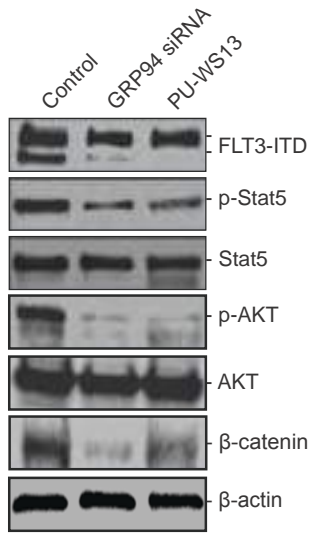
C



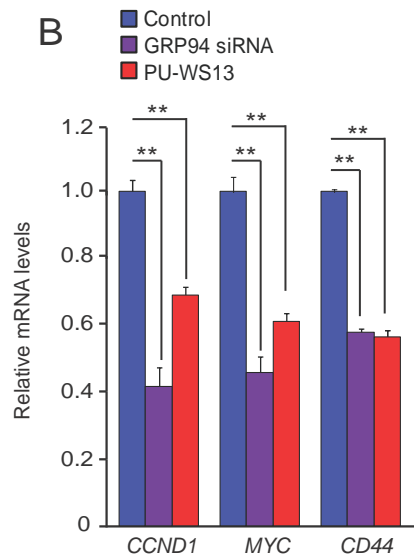




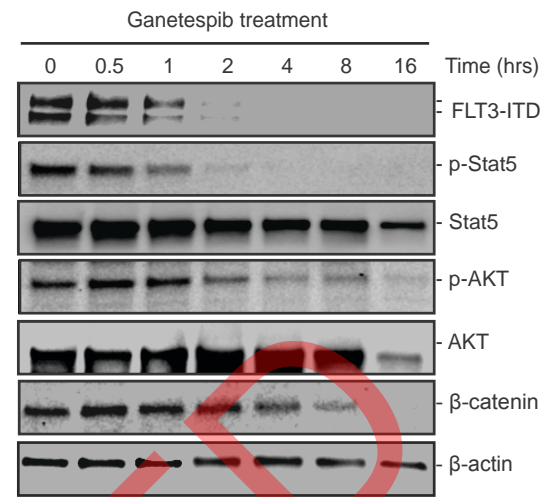
A



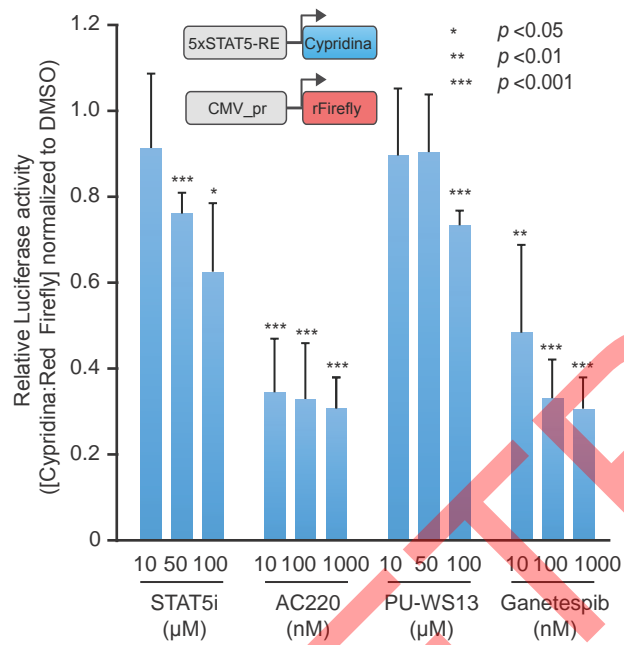
B



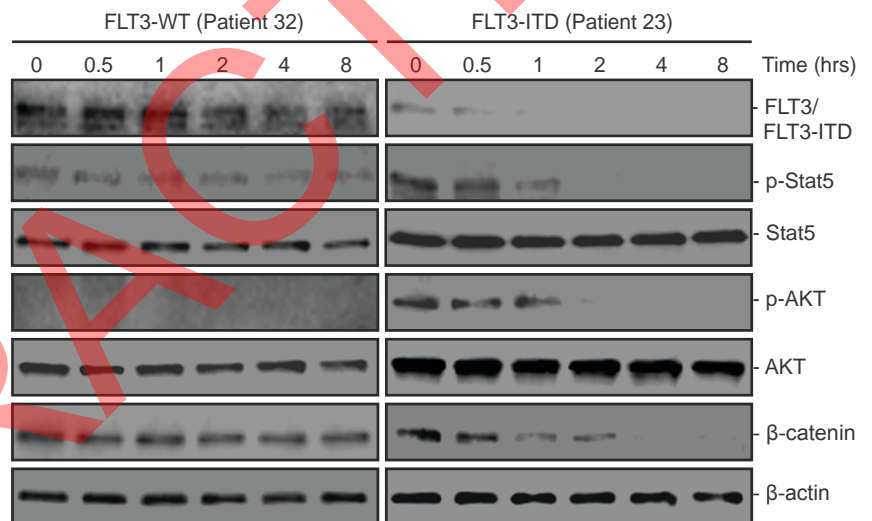
C

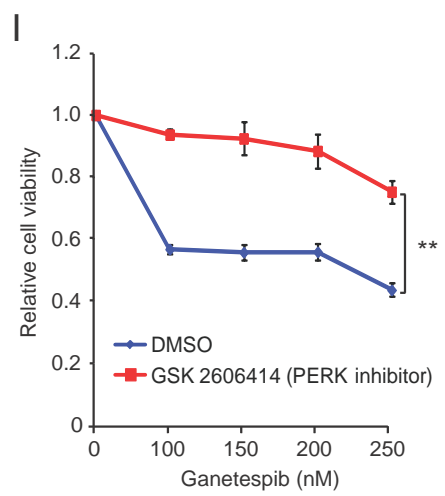
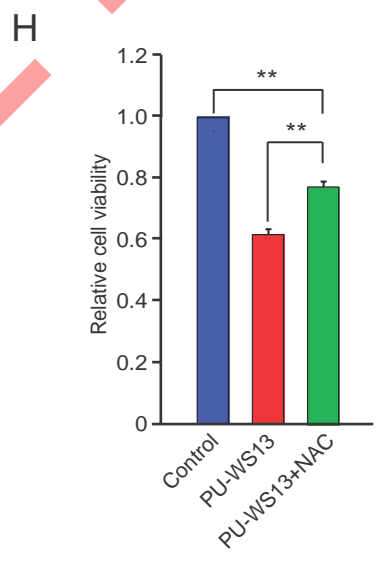
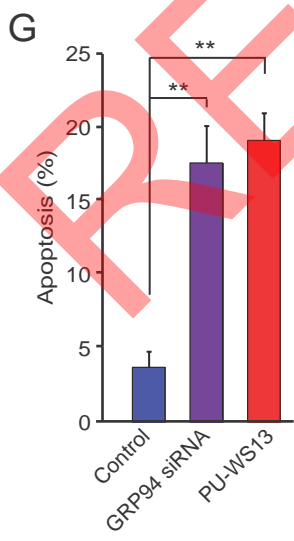
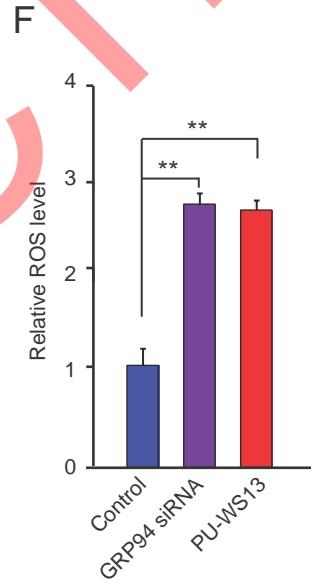
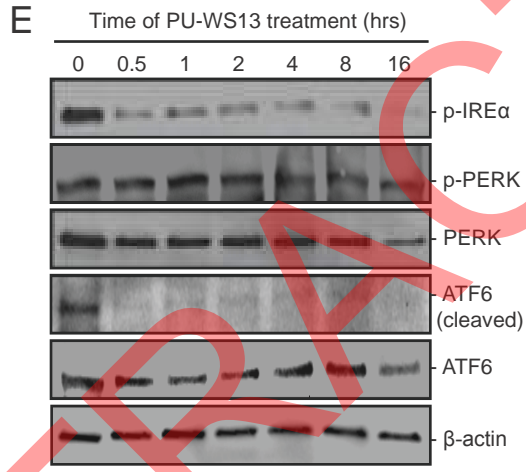
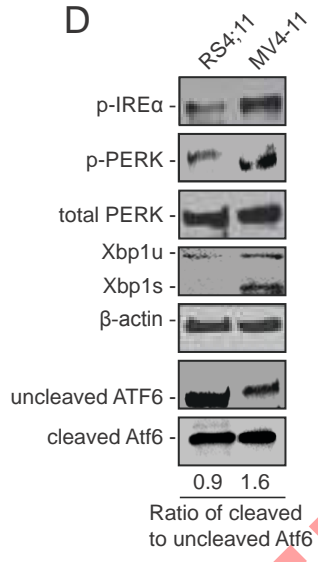
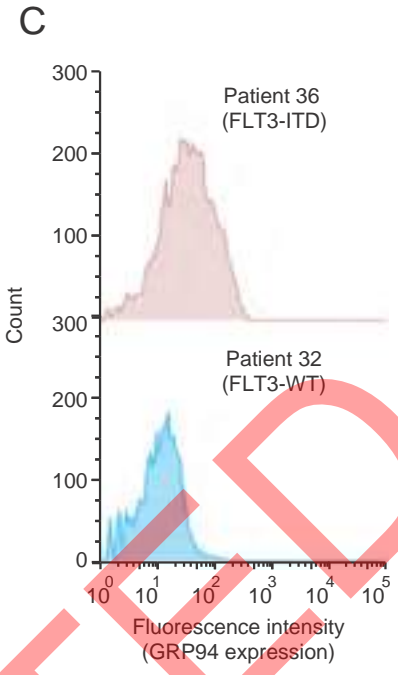
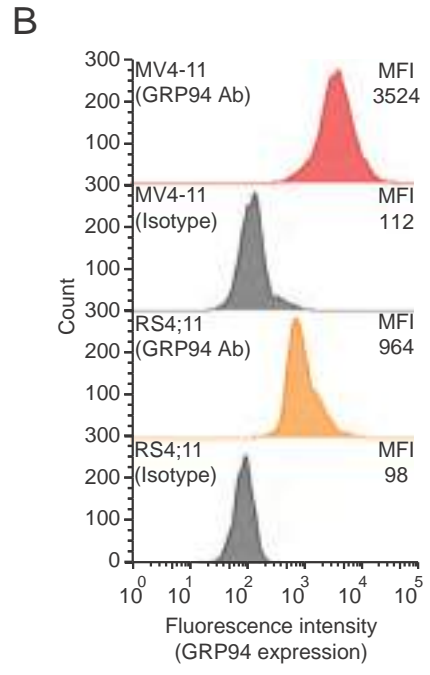
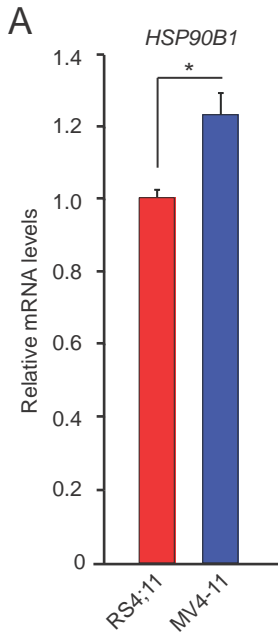


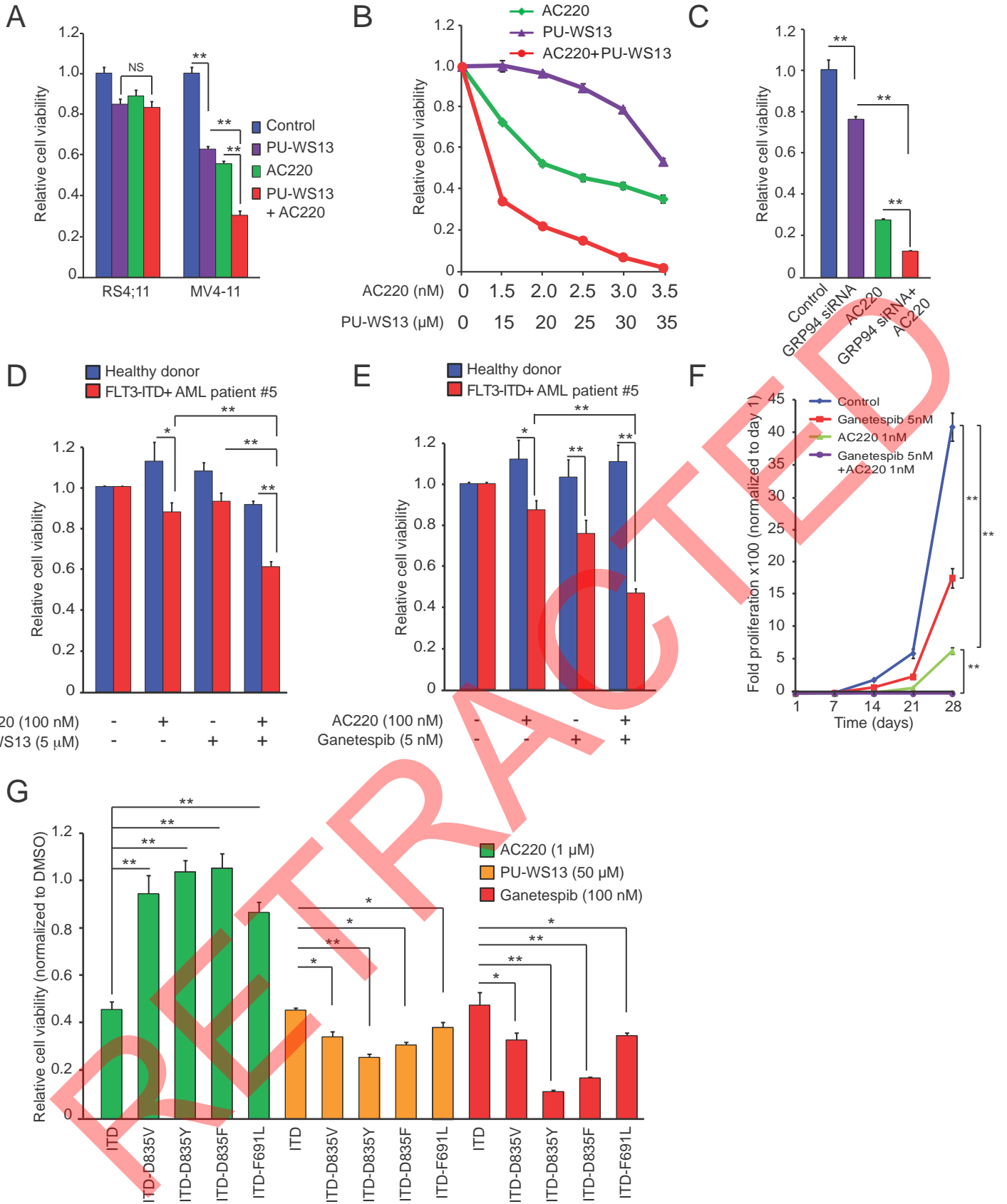
D

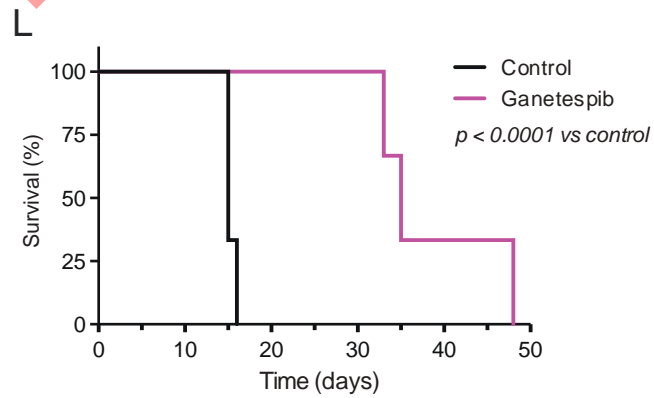
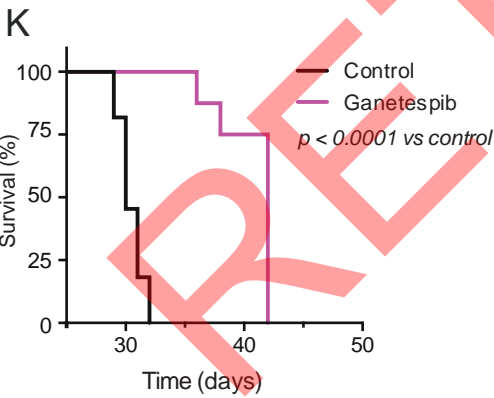
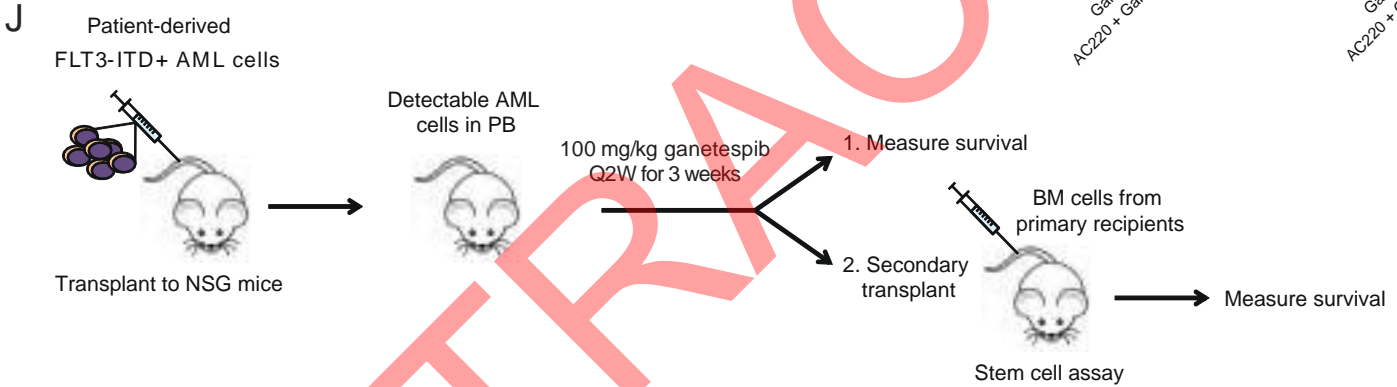
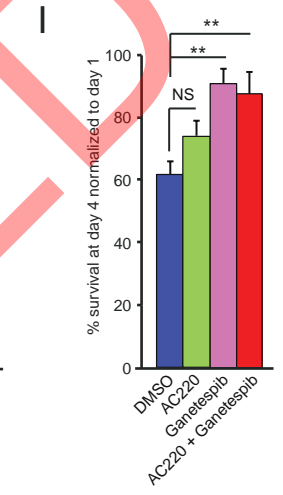
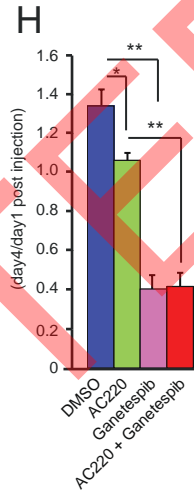
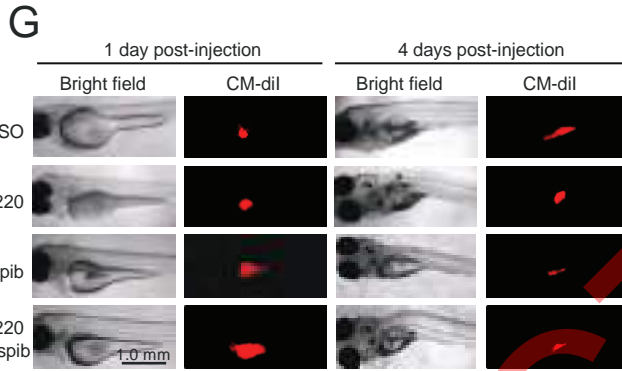
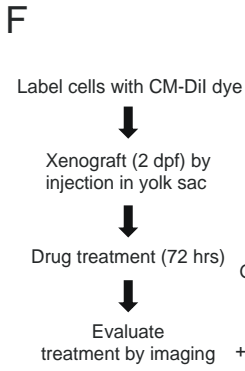
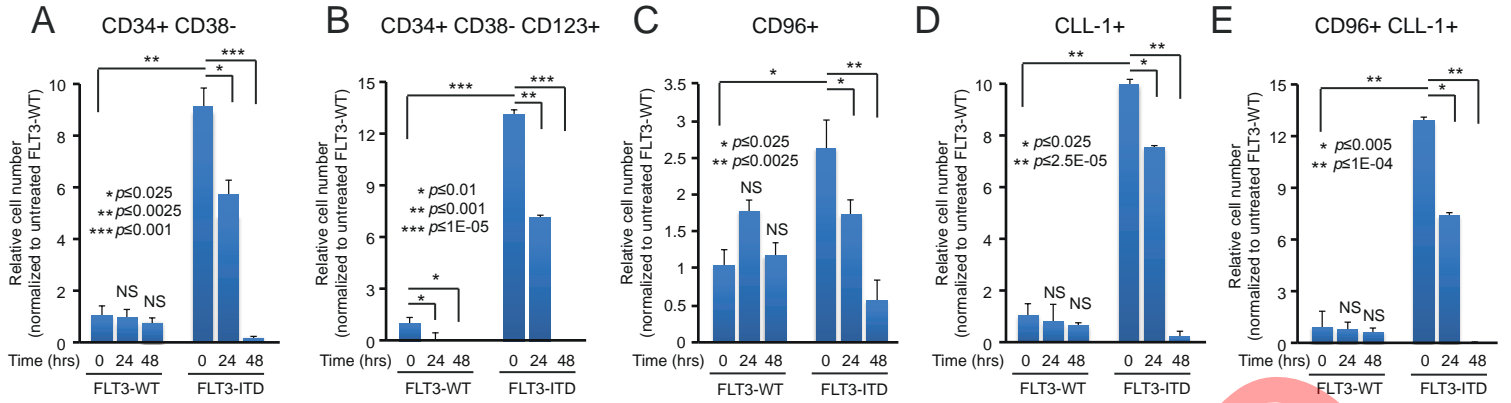


E

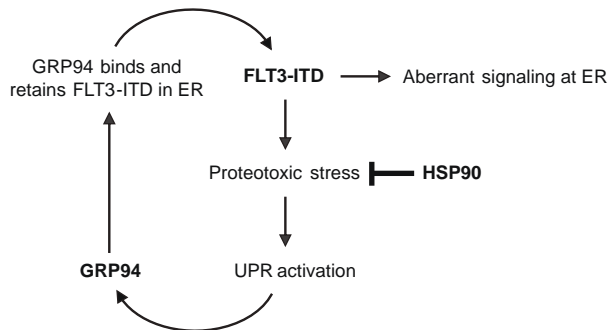




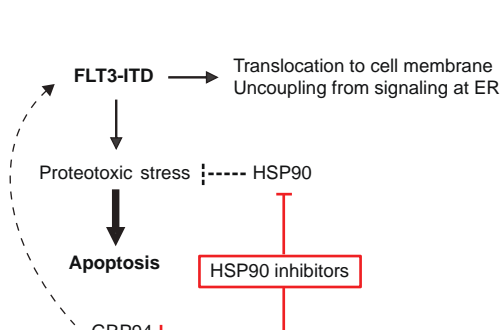




**M** GRP94-dependent nefarious feedback loop



**N** HSP90 inhibitors break feedback loop



## Supplementary Data

### Supplementary Figure legends

**Supplemental Figure S1. FLT3-ITD+ and FLT3-TKD+ AML cells are highly sensitive to HSP90 inhibitors.** *A*, Magnification of part of Figure 1A. *B-D*, FLT3-ITD+ and FLT3-TKD+ AML cells are significantly more sensitive to HSP90 inhibitors than FLT3-WT AML cells or BM-derived cells from healthy donors. Cell survival in response to high doses (indicated above the graphs) of the HSP90 inhibitors ganetespib (B,C) and luminespib (D,E).

**Supplemental Figure S2. FLT3-ITD is retained in the ER as an immature protein.** *A*, FLT3-ITD interacts with Calnexin. Proteins were immunoprecipitated from RS4;11 cells (FLT3-WT) or MV4-11 cells (FLT3-ITD) using either anti-Calnexin or anti-FLT3 antibodies and copurifying proteins were analyzed by Western blotting. *B*, FLT3-ITD localizes to the ER. MV4-11 cells were fixed and stained with DAPI, anti-Calnexin and anti-FLT3 antibodies, followed by fluorescence microscopy imaging. *C*, FLT3-ITD localizes to intracellular compartments in Ba/F3 cells. Ba/F3 cells stably transfected with FLT3-WT and FLT3-ITD were fixed and stained with DAPI and anti-FLT3 antibodies, followed by imaging using fluorescence microscopy. *D*, FLT3-ITD is expressed as an immature protein. FLT3 and FLT3-ITD were immunoprecipitated from RS4;11 cells and from MV4-11 cells, respectively, and treated with either Peptide-*N*-Glycosidase F (PNGase F), which cleaves all oligosaccharides from *N*-linked glycoproteins, or with Endoglycosidase H (Endo H), which primarily cleaves high mannose sugars from *N*-linked glycoproteins. FLT3 glycosylation was analyzed by Western blotting using FLT3 antibodies. *CG*, complex glycosylated FLT3; *HM*, high mannose FLT3; *DG*, deglycosylated FLT3. *E*, *F*, FLT3-ITD kinase inhibits receptor maturation. MV4-11 cells (*E*) or RS4;11 cells (*F*) were treated with either 100 ng/ml FLT3 ligand (FLT3L) or with 1  $\mu$ M AC220, after which receptor maturation and stability was



monitored by Western blotting. **G**, Inhibition of FLT3-ITD kinase activity results in translocation of the receptor from the ER to the cell membrane. Cells were treated as in (E) after which FLT3 and the cell membrane were imaged as in (C).

**Supplemental Figure S3. Inhibition of HSP90 family proteins results in maturation and cell membrane translocation of FLT3-ITD.** **A**, Cell surface localization of FLT3-ITD in living, unpermeabilized MV4-11 cells. FLT3-ITD cell surface localization was analyzed by flow cytometry after treatment with DMSO, AC220 (100 nM), PU-WS13 (50  $\mu$ M), or Ganetespib (100 nM) for 24 hrs. **B**, MV4-11 cells were treated with 50  $\mu$ M PU-WS13 for the indicated times, after which FLT3 maturation was monitored by altered mobility on SDS-PAGE followed by Western blotting with FLT3 antibodies. **C**, PU-WS13 treatment induces cell surface translocation of FLT3-ITD in Ba/F3 cells. Ba/F3 cells stably expressing FLT3-WT or FLT3-ITD were treated with 50  $\mu$ M PU-WS13 for 24 hrs after which FLT3 localization was analyzed as in Fig. 3A. **D**, Ganetespib treatment induces cell surface translocation of FLT3-ITD. MV4-11 cells were treated with 100 nM ganetespib for 24 hrs after which FLT3 localization was analyzed as in Fig. 3A. **E,F**, GRP94 protein levels after siRNA knockdown or treatment with PU-WS13.

**Supplemental Figure S4. GRP94 reduces ROS levels and protects FLT3-ITD-expressing cells from apoptosis.** **A**, Inhibition of FLT3-ITD results in decreased GRP94 protein levels. MV4-11 cells were treated with AC220 (100 nM) for 24 hrs. GRP94 protein levels were analyzed by flow cytometry using permeabilized MV4-11 cells and GRP94-specific antibodies. MFI, median fluorescence intensity. Three independent experiments were performed. Error bars, SEM. \*\*,  $p < 0.01$ . **B**, Increased GRP94 protein expression levels in primary FLT3-ITD+ AML cells compared with BM cells from a healthy donor. **C**, Increased

ROS levels in FLT3-ITD-expressing cells. ROS levels were visualized in RS4;11 and MV4-11 cells by fluorescence microscopy and the data were quantified as described in the Methods. Three independent experiments were performed. Error bars, SEM. \*\*,  $p < 0.01$ . **D**, Increased UPR activity in primary FLT3-ITD+ AML cells relative FLT3-WT primary AML cells. **E**, Increased UPR activity in Ba/F3 cells expressing FLT3-ITD relative to Ba/F3 cells expressing FLT3-WT. **F**, Inhibition of HSP90 diminishes IRE1 and ATF6 but not PERK. MV4-11 cells were treated with 100 nM ganetespib, after which cell lysates were analyzed with the indicated antibodies. **G**, Inhibition of GRP94 diminishes IRE1 and ATF6 but not PERK in FLT3-ITD-expressing Ba/F3 cells. Cells were treated with 50  $\mu$ M PU-WS13 and analyzed as in (F). **H**, Inhibition of GRP94 diminishes IRE1 and ATF6 but not PERK in primary FLT3-ITD+ AML cells. Cells were treated with 50  $\mu$ M PU-WS13 for 4 hrs and analyzed as above. **I**, Inhibition of HSP90 inactivates IRE1 and Atf6 but not PERK only in AML cells. Healthy control cells (left panel) or cells from an FLT3-ITD+ AML patient (right panel) were treated with 100 nM ganetespib after which cell lysates were analyzed by Western blotting with the indicated antibodies. **J-L**, Inhibiting GRP94 induces apoptosis. GRP94 was inhibited by siRNA depletion or by treatment with PU-WS13 and apoptotic MV4-11 cells were visualized by TUNEL assay (J), or analyzed by flow cytometry using Annexin V staining (K) or propidium iodide (L). **M**, Treatment with NAC reduces PU-WS13-induced ROS levels. MV4-11 cells were treated with DMSO, 50  $\mu$ M PU-WS13, or PU-WS13 combined with 5 mM NAC as indicated, after which ROS levels were quantified by flow cytometry.

**Supplemental Figure S5. PU-WS13 synergizes with AC220.** **A-D**, Visualization of the synergy index of MV4-11 cells treated for 2 days with the indicated combinations of PU-WS13 and AC220 with SynergyFinder using ZIP (A), Bliss (B), Loewe (C) and HSA (D) models. **E**, FLT3-ITD+ AML cells are more sensitive to a combination of AC220 and

ganetespib than FLT3-WT AML cells. Primary patient cells were incubated with 100 nM ganetespib in combination with increasing doses of AC220 as indicated in the figure, and cell viability was analyzed by CellTiter-Glo after 72 hrs.

**Supplemental Figure S6. Ganetespib and AC220 selectively inhibit FLT3-ITD+ AML cells in a zebrafish xenograft model.** **A**, Inhibition of MV4-11 cell viability by ganetespib and AC220. Transplanted fish were treated and analyzed as described in Fig. 7G. **B**, Quantification of the data shown in (A). Error bars, SEM. \*,  $p < 0.05$ ; \*\*,  $p < 0.01$ . **C**, FLT3-ITD+ AML patient cells often spread through the fish and are inhibited by ganetespib. Fish were transplanted, treated and analyzed as described in Fig. 7G. **D**, Ganetespib promotes survival of zebrafish xenografted with FLT3-ITD+ AML patient cells shown in (C). Error bars, SEM. \*,  $p < 0.05$ . **E**, Healthy donor BM cells are not affected by ganetespib or AC220. Transplanted fish were treated and analyzed as described in Fig. 7G. **F**, Quantification of the experiment shown in (E). **G**, Ganetespib has little or no effect on xenografted blast cells from FLT3-WT patient cells. Transplanted fish were treated and analyzed as described in Fig. 7G. **H**, Quantification of the experiment shown in (G). 10-15 fish were analyzed for each treatment and three independent experiments were performed. Error bars, SEM. NS, not significant.

## **Supplemental Table legends**

**Supplemental Table S1.** The library of compounds used for *ex vivo* drug screening.

**Supplemental Table S2.** Information of AML patients.

**Supplemental Table S3.** MS data for the FLT3 pulldown experiments using RS4;11 and MV4-11 cells.

RETRACTED

## Supplementary methods

### *Ex vivo drug sensitivity screening*

Drug sensitivity screening was basically performed as described previously <sup>1</sup>. Bone marrow aspirates or peripheral blood samples were obtained from six healthy donors and 41 AML patients. Mononuclear cells were isolated using a Ficoll density gradient (Lymphoprep™, STEMCELL Technologies Inc.). Cells were suspended in Mononuclear Cell Medium (MCM; PromoCell) supplemented with 100 units/mL of penicillin and 100 µg/mL of streptomycin. The cells were then treated with a collection of compounds using the Selleck Anti-cancer Compound Library containing 349 anti-cancer compounds (Suppl. Table S1), which includes many FDA/EMA-approved drugs as well as compounds in various stages of clinical trials (Suppl. Table S1). All compounds were dissolved in DMSO and dispensed in 384-well microplates (Greiner Bio-One) using an Echo 550 (Labcyte Inc.) acoustic liquid handling device at the Biotechnology Centre of Oslo. Each compound was tested in five different concentrations covering a 10,000-fold concentration range (1–10,000 nM), except for VPA (100 nmol/L to 1 mmol/L). In general, 10,000 cells in a volume of 25 µL were added to each well using a Multi Drop Combi peristaltic dispenser (Thermo Scientific). In some cases, when the cell count was low, less cells (typically 2,000–5,000, in one case 600) were dispensed per well without noticeable differences in experimental outcome. The plates were incubated for 72 hours at 37°C with 5% CO<sub>2</sub> in a humidified environment. Cell viability was estimated using CellTiter-Glo luminescent assay (Promega) according to the manufacturer's instructions using an EnVision 2104 Multilabel plate reader (Perkin Elmer). The readouts were normalized to negative (DMSO) and positive (100 µmol/L benzethonium chloride) control wells and analyzed as described below.

### *Dose-response curve fitting and clusters*

To evaluate the impact of each drug on the viability of the cells, the area under the relative viability curve (AUC) was calculated as previously described <sup>2</sup>, and defined by the sum of normalized measures (relative viability) at all tested concentrations of the drug. As each drug is tested at five different concentrations, AUC = 5 corresponds to an inactive compound and smaller values to compounds inducing cell death. In order to select drugs killing specifically patient cells compare to healthy donor cells, we used for each drug the measure SPA (specific area) = “average (AUC healthy donors) – AUC<sub>patient</sub>”. Thus, high SPA values indicate drugs that selectively inhibit patient cells but not healthy donor cells. The SPA values were then used to cluster the drugs and patients using Euclidian distance measures. Heatmaps were generated using the d3Heatmap package (<https://cran.r-project.org/web/packages/d3heatmap/index.html>) on R software.

### *Drug Hunter app*

The Drug Hunter analysis app was developed in R (<http://www.R-project.org/>) using the Shiny framework (<https://CRAN.R-project.org/package=shiny>) to enable instantaneous analysis of survival assay results and comparison with other patients. An alpha version of the software, with future development plans is available as a public repository on GitHub (<https://github.com/adrowe1/Drug-Hunter>). Cross-referencing plate-reader data with drug library titration coordinates allows immediate visualization of raw data, drug response fingerprints for a single patient compared to healthy donors, interactive filtering and selection of drug subgroups classified by response, and additional annotation of datasets with drug target metadata. Individual datasets may then be aggregated to investigate clustering of drug responses by disease type, or other patient-specific classification data such as mutational analyses.

### *Reagents and Antibodies*

AC220/quizartinib (Selleckchem, Munich, Germany), PU-WS13 (BioVision, Milpitas, USA), GSK2606414, Stat5 inhibitor (*N'*-((4-oxo-4H-chromen-3-yl)methylene)nicotinohydrazide)), ganetespib and NVP-AUY922 (Santa Cruz biotechnology, Santa Cruz, USA) were all prepared in stock solution of 10 mM in DMSO. Hoechst 33342 Solution (Thermo Fisher Scientific, Waltham, USA) was used for nuclear staining and N-Acetyl-L-cysteine (NAC) was obtained from Sigma Aldrich. Recombinant Human Flt3-Ligand was purchased from PeproTech Nordic (Stockholm, Sweden). The following antibodies were used: Rabbit anti-beta actin (Abcam, Cambridge, United Kingdom), Mouse anti-FLT3 (R&D Systems, Minneapolis, USA), Rabbit anti-FLT3 (Santa Cruz), Rabbit anti-Hsp90 (Abcam), Rabbit anti-Calnexin (Sigma Aldrich), IgG from rabbit serum (Sigma Aldrich), Rabbit anti-GRP94 Antibody (Abcam), Rabbit anti-Stat5 (Cell signaling, Danvers, USA), Rabbit anti-Phospho-Stat5 (Tyr694) (Cell signaling), Rabbit anti-Phospho-AKT (Thr308) (Cell signaling), Rabbit anti-AKT (Cell signaling), Rabbit anti-beta catenin (Santa Cruz), Rabbit anti-Xbp1 (Abcam), Rabbit anti- Phospho-IRE1 alpha (Ser724) (R&D Systems), Rabbit anti-Phospho-PERK Antibody (Thr 981) (Santa Cruz), Rabbit anti-PERK Antibody (Santa Cruz), Rabbit anti-ATF6 (Abcam), Mouse anti-CD34 antibody (FITC) (Abcam), Mouse anti-CD38 antibody (Phycoerythrin) (Abcam), Mouse anti-IL3RA antibody (PerCP/Cy5.5) (Abcam), Mouse anti-CD96 antibody (Abcam), Rabbit-anti-COLEC10 antibody (Abcam), Goat anti-Rabbit IgG-HRP (GE healthcare, Chicago, USA), Goat anti-mouse IgG/IgM-HRP (Abcam), Goat Anti-Rabbit IgG H&L (Alexa Fluor 488) and Goat Anti-Mouse IgG H&L (Alexa Fluor 555) (Abcam).

### *Detection of glycoproteins*

Protein glycosylation was analyzed by digestion with PNGase F or Endo H N-glycosidase (New England Biolabs, Ipswich, United States) according to the manufacturer's instructions.

#### *Flow cytometry*

Protein expression levels were measured by flow cytometry. Briefly, cells with or without permeabilization were harvested and washed 3 times in PBS buffer. Unspecific staining was blocked by incubation in 0.5% BSA blocking buffer for 30 min at 37°C. Primary antibodies were added for 45 min, followed by washing 3 times with PBS and staining for 30 min with fluorophore-conjugated secondary antibodies at 37°C. After washing 3 times, the cells were analyzed by FACS Aria flow cytometry (BD Biosciences, San Jose, USA) according to the manufacturer's instructions.

#### *Luciferase assays*

Ba/F3 cells were stably transfected with pCMV-Red Firefly Luc Vector (Life technologies) and pLuc Mini-TK 2 vector (New England Biolabs) containing luciferase under the control of 5 copies of the STAT5 response element, as well as pLKO.1-blast-FLT3-ITD vector (kindly provided by Prof. C. Réher). Cells were treated with the test compounds and luciferase assays were carried out using the Pierce Cypridina-Firefly Luciferase Dual Assay Kit (Life technologies) according to the manufacturer's instructions.

#### *Intracellular ROS measurements*

Intracellular ROS status was measured using Cell ROX Green Reagent (Life technologies). The cells were treated with 5 µM reagent for 30 min at 37 °C in 5% CO<sub>2</sub>, and washed 3 times with PBS. Following nuclear staining by 40 mg/ml Hoechst 33342 solution (Thermo Fisher Scientific) for 3 min, the images were captured using the Flouid cell imaging station (Life



technologies) and analyzed by the Image J software. ROS fluorescence signals were also analyzed by FACS Aria flow cytometry according to the manufacturer's instructions.

#### *Detection of apoptotic cells*

Apoptotic cells were visualized using the Deadend Colorimetric TUNEL System (Promega) according to the manufacturer's instructions and the images were captured using the Fluid cell imaging station. Apoptotic cells were also detected by flow cytometry using the Alexa Fluor 488 Annexin V/Dead cell apoptosis Kit (Life technologies) according to the manufacturer's instructions.

#### *Cell cycle analysis*

In brief,  $1 \times 10^5$  cells were washed twice with ice-cold PBS and suspended in 70% ethanol for at least 2 hours at 4°C. The cells were then centrifuged for 5 min at 300g and resuspended in 1 ml Propidium Iodide (PI) (Thermo Fisher Scientific, Waltham, USA) staining solution (0.1% Triton-X100, 10 µg/ml PI and 100 µg/ml DNase free RNase A in PBS) and kept in the dark for 5 min at 37°C before analysis by flow cytometry.

#### *Total RNA extraction, cDNA synthesis, and RT-qPCR*

RNA was extracted using the RNeasy Mini kit (Qiagen, Hilden, Germany) according to the manufacturer's instructions. cDNA was synthesized using the SuperScript III cDNA synthesis kit (Life Technologies) with random primers (Life Technologies). RT-qPCR was performed using Power SYBR Green Master Mix (Applied Biosystems, Foster City, USA) and the Step One Plus Real-time PCR system (Applied Biosystems, Foster City, USA). The primers for amplifying the target genes are shown as follows: hs *ACTB* Forward: 5'-TGTGCTATCCCTGTACGCCTC-3', Reverse: 5'-GTAGATGGGCACAGTGTGGGTGA-3';

hs *CCND1*: Forward: 5'-TCTACACCGACAACCTCCATCCG-3', Reverse: 5'-  
TCTGGCATT TTTGGAGAGGAAGTG-3'; hs *c-MYC*: Forward: 5'-  
AATGAAAAGGCCCCCAAGGTAGTTATCC-3'; Reverse: 5'-  
GTCGTTTCCGCAACAAGTCCTCTTC-3'; hs *CD44*: Forward: 5'-  
GCTTCTCTACATCACATGAAGGCTT-3'; Reverse: 5'-  
CTCCACCTGTGACATCATTCCT-3'.

#### *Immunoprecipitation and immunoblotting assays*

Cells were washed 3 times with ice-cold PBS and lysed in lysis buffer (20 mM Tris-HCl, pH 8.0, 250 mM NaCl, 2 mM EDTA, 10% glycerol, 1% NP-40, 1% Protease Inhibitor Cocktail, 1 mM PMSF). After incubation for 30 min on ice, lysates were centrifuged at 15 000 g for 10 min and pellets were discarded. Lysates were immunoprecipitated with primary antibodies for 2 hours at 4°C. Subsequently, antibodies were collected with protein A beads (Thermo Scientific) and the mixture was rocked overnight at 4°C. The beads were then washed 3 times with cold lysis buffer and analyzed by mass spectrometry, and a small part of the sample was also analyzed by SDS-PAGE followed by Western blotting. After boiling for 5 min at 95 °C, SDS solution was collected, separated by SDS-PAGE and electro-blotted onto nitrocellulose membranes (Bio-Rad, Hercules, USA). The membranes were blocked in buffer consisting of TBS-T (0.1% Tween-20) containing 5% milk for 30 min. Subsequently, primary antibodies were added and incubated overnight at 4°C, washed 3 times with TBS-T buffer, and incubated with HRP-labeled secondary antibodies at room temperature for 1 h. After 3 washes with TBS-T, the membranes were incubated in Pierce ECL western blotting substrate (Thermo Scientific) and visualized using a Molecular Imager Gel Doc XR+System with Image Lab Software (Bio-Rad).

### *Protein-protein interaction networks*

We used the Search Tool for the Retrieval of Interacting Genes/Proteins (STRING) database<sup>3</sup> to visualize the physical and functional protein-interaction properties of the chaperone network of FLT3-ITD. Proteins identified by MS to preferentially interact with FLT3-ITD were first analyzed by Gene Ontology (GO-Slim Biological Process) using PANTHER<sup>4</sup>, and proteins with molecular chaperone functions were uploaded to the STRING database to generate the protein-protein interaction network. The stroke of the edges represents the confidence score of a functional association, which was calculated based on co-expression, experimental and biochemical validation, association in curated databases, and co-occurrence in the literature<sup>3</sup>.

### *Zebrafish xenograft, imaging and analysis*

The Casper strain of zebrafish (*Danio rerio*) was used in accordance with the guidelines established by the committee of Animal Welfare and Management for experiments in Oslo University Hospital. In brief, 48 hrs post fertilization (hpf) zebrafish were anesthetized with 2-phenoxyethanol solution (100 ppm; Sigma Aldrich) and arrayed on a holding sheet. Cells were labeled by CM-DiI dye (Thermo Fisher Scientific) according to the manufacturer's instructions and suspended in Hanks' balanced salt solution (Thermo Fisher Scientific) at 20 000 cells/ $\mu$ l, and 100-200 cancer cells were injected into the avascular region of the yolk sac in each zebrafish by the glass needles and the FemtoJet injection system (Eppendorf, Hamburg, Germany). After xenografts, zebrafish were transferred from 28°C to 32°C. We evaluated the leukemia xenografts by fluorescence microscopy (ZEISS, Oberkochen, Germany) at 24 hours post injection (hpi) before drug treatment. The fish were transferred into 24-well plates with the test drugs, which were replaced daily. After 72 h treatments, the fish were imaged again and the area or density of fluorescent cells was analyzed with Image J

software. Finally, all the zebrafish were killed by an overdose of anesthesia upon conclusion of the experiments.

## References

1. Pemovska T, Kontro M, Yadav B, et al. Individualized systems medicine strategy to tailor treatments for patients with chemorefractory acute myeloid leukemia. *Cancer Discov.* 2013;3(12):1416-1429.
2. Fallahi-Sichani M, Honarnejad S, Heiser LM, Gray JW, Sorger PK. Metrics other than potency reveal systematic variation in responses to cancer drugs. *Nat Chem Biol.* 2013;9(11):708-714.
3. Szklarczyk D, Franceschini A, Wyder S, et al. STRING v10: protein-protein interaction networks, integrated over the tree of life. *Nucleic Acids Res.* 2015;43(Database issue):D447-452.
4. Mi H, Huang X, Muruganujan A, et al. PANTHER version 11: expanded annotation data from Gene Ontology and Reactome pathways, and data analysis tool enhancements. *Nucleic Acids Res.* 2017;45(D1):D183-D189.

Fig. S1

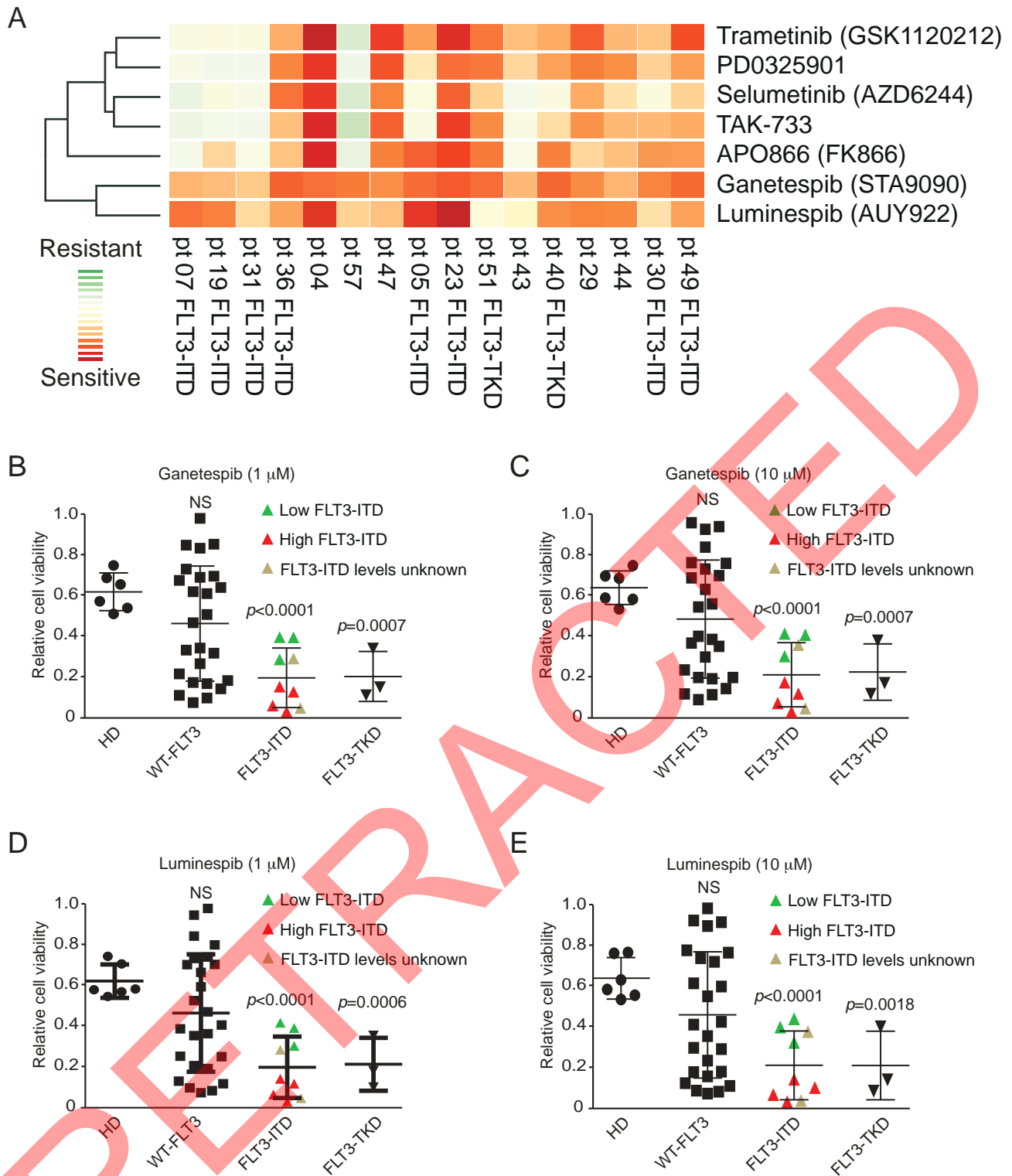


Fig. S2

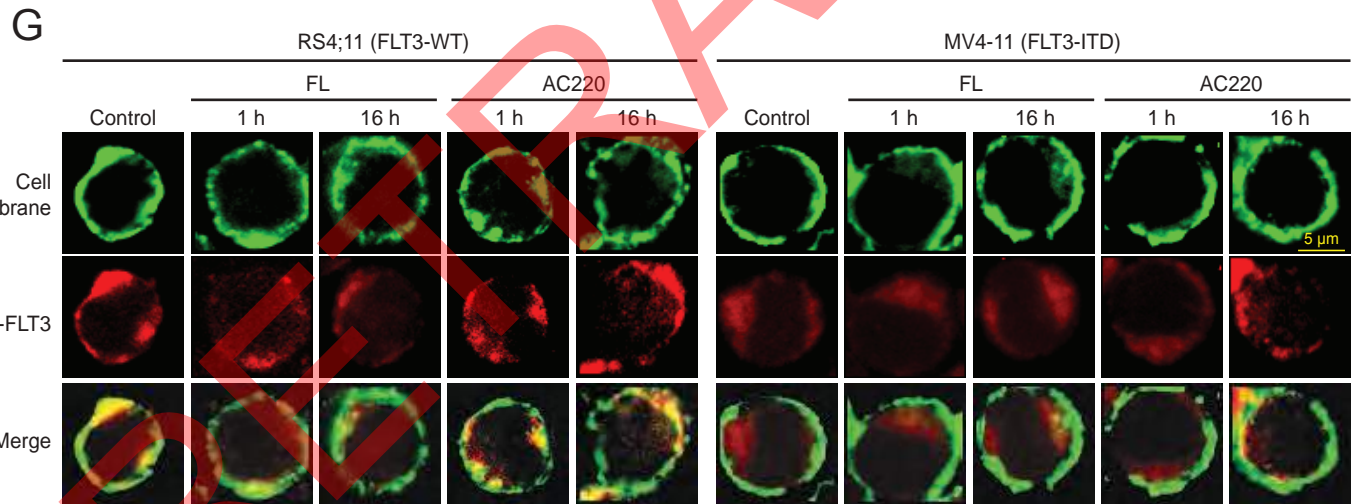
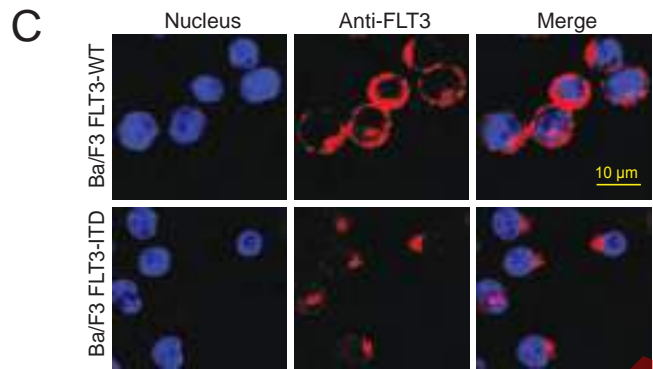
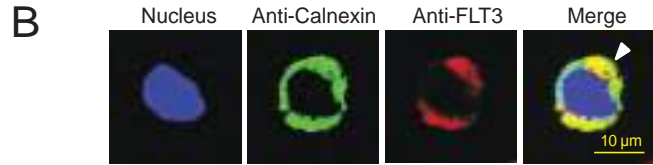
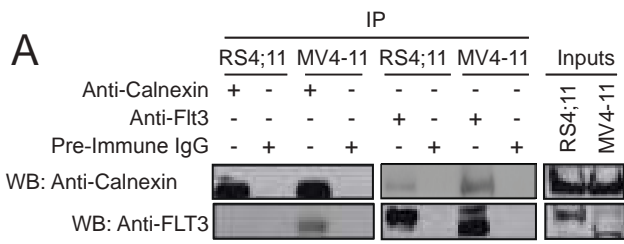
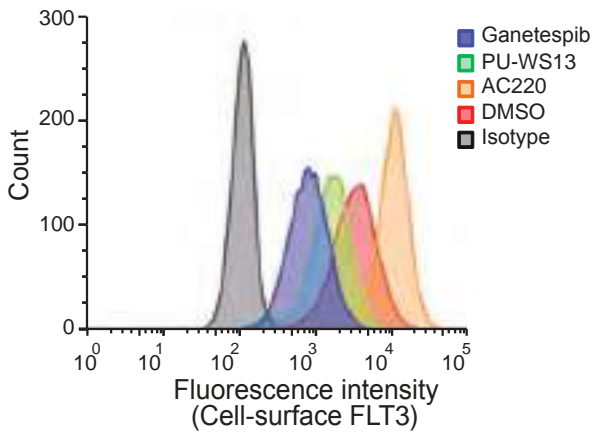
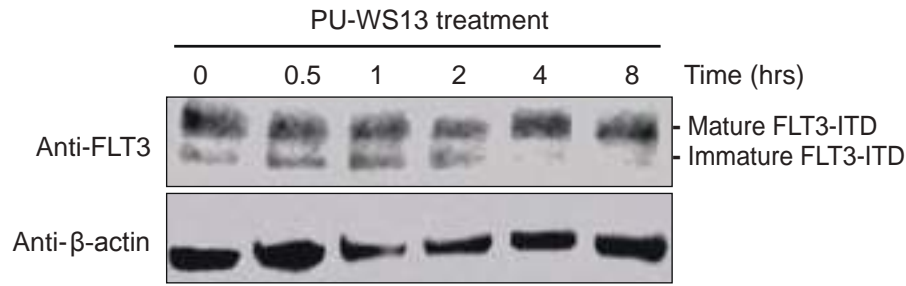


Fig. S3

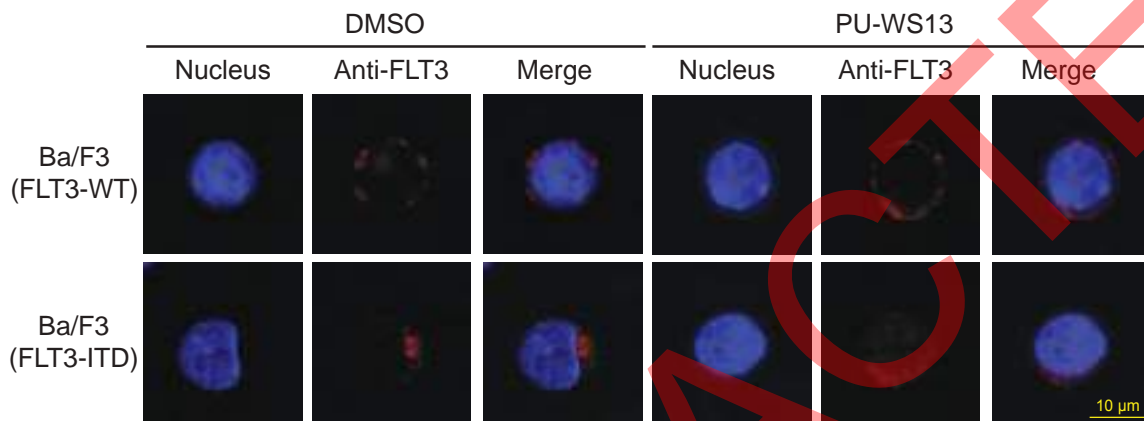
A



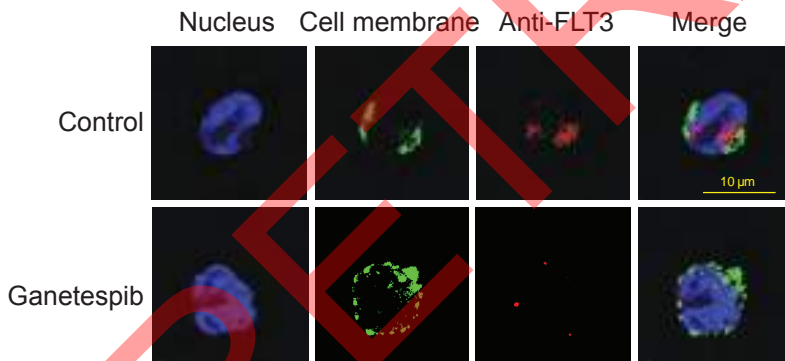
B



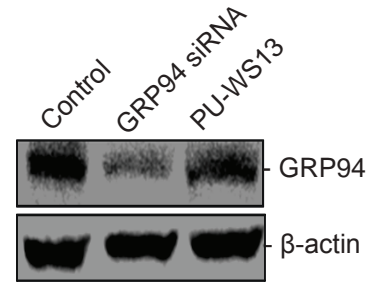
C



D



E



F

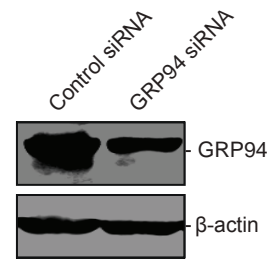


Fig. S4

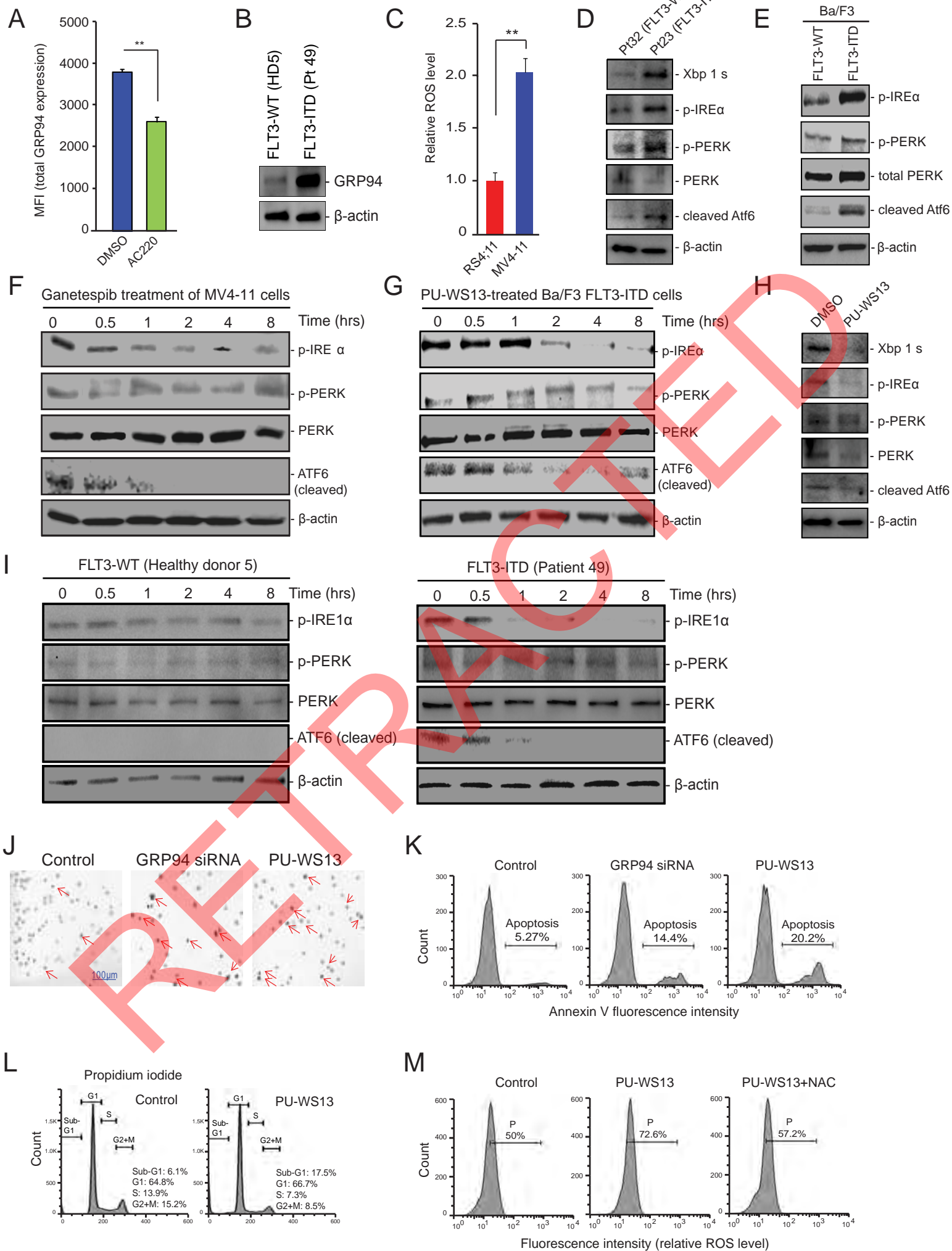
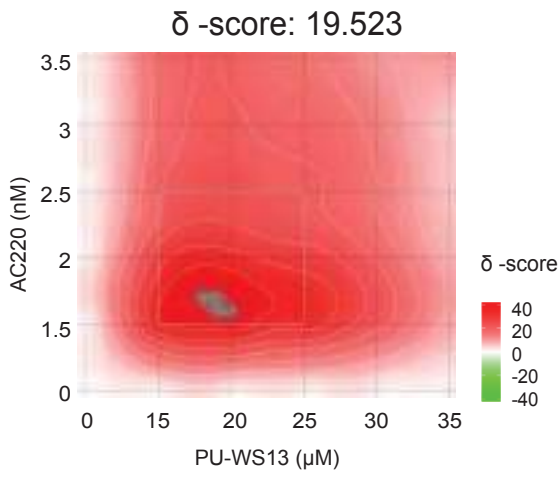




Fig. S5

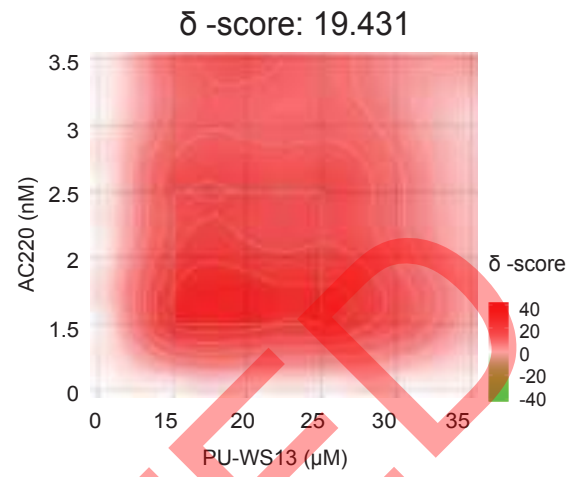
A

ZIP model



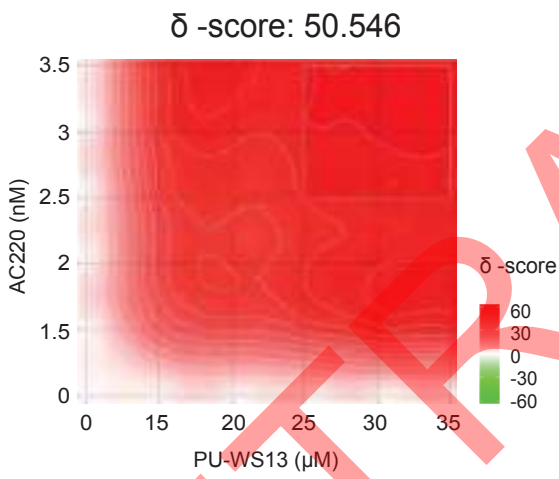
B

Bliss model



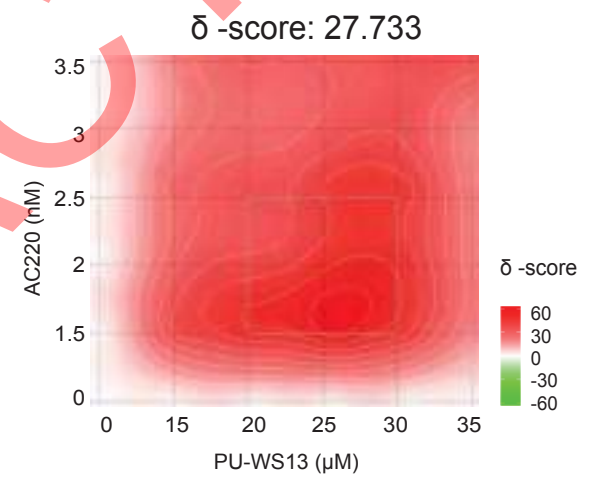
C

Loewe model



D

HSA model



E

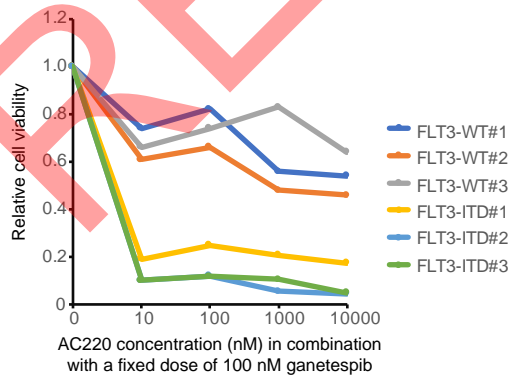


Fig. S6

